

See discussions, stats, and author profiles for this publication at: <https://www.researchgate.net/publication/267267764>

Carboxyl-Catalyzed Prototropic Rearrangements in Histidine Peptide Radicals upon Electron Transfer: Effects of Peptide Sequence and Conformation

ARTICLE *in* JOURNAL OF THE AMERICAN CHEMICAL SOCIETY · JANUARY 2009

Impact Factor: 12.11

CITATIONS

3

READS

16

9 AUTHORS, INCLUDING:



[Subhasis Panja](#)

National Physical Laboratory - India

50 PUBLICATIONS 821 CITATIONS

[SEE PROFILE](#)



[Anneli Ehlerding](#)

Swedish Defence Research Agency

67 PUBLICATIONS 1,084 CITATIONS

[SEE PROFILE](#)



[Steen Brøndsted Nielsen](#)

Aarhus University

197 PUBLICATIONS 3,073 CITATIONS

[SEE PROFILE](#)



[Preben Hvelplund](#)

Aarhus University

58 PUBLICATIONS 1,000 CITATIONS

[SEE PROFILE](#)

Carboxyl-Catalyzed Prototropic Rearrangements in Histidine Peptide Radicals upon Electron Transfer: Effects of Peptide Sequence and Conformation

František Tureček,* Subhasis Panja, Jean A. Wyer, Anneli Ehlerding, Henning Zettergren, Steen Brøndsted Nielsen, Preben Hvelplund, Benjamin Bythell, and Béla Paizs

Department of Chemistry, Bagley Hall, Box 351700, University of Washington, Seattle, Washington 98195-1700, Department of Physics and Astronomy, Aarhus University, Aarhus, Denmark, and Department of Molecular Biophysics, German Cancer Research Center, Im Neuenheimer Feld 580, D-69120 Heidelberg, Germany

Received June 18, 2009; E-mail: turecek@chem.washington.edu

Abstract: We report an unusual prototropic rearrangement in gas-phase radicals formed by collisional electron transfer from cesium atoms to protonated peptides HAL, AHL, and ALH at 50 keV. The rearrangement depends on the peptide amino acid sequence and presence or steric accessibility of a free carboxyl group. Upon electron transfer, protonated HAL and ALH rearrange to tautomers that are detected as nondissociated anions in charge-reversal mass spectra. The isomerization is minor in protonated ALH and virtually absent in HAL amide. Electron structure calculations indicate that the gas-phase ions are preferentially protonated in the His imidazole ring and consist of multiple conformers that differ in their hydrogen bonding patterns. Electron transfer to protonated HAL and AHL triggers an exothermic and dynamically barrierless transfer of the carboxyl proton onto the C-2' position of the His ring that occurs on a 120–240 ns time scale. The kinetics of this isomerization are controlled by internal rotations in the radicals to assume conformations favoring the proton transfer. The radical conformations also affect subsequent proton migrations in zwitterionic His imidazoline intermediates that reform the COOH group and result in His ring isomerization. This autocatalytic prototropic rearrangement in gas-phase peptide radicals is analogous to enzyme catalytic reactions involving His and acidic amino acid residues. In contrast to HAL and AHL, the C-2' position is sterically inaccessible in ALH radicals. These radicals undergo proton migrations to the His ring C-5' positions that have moderate energy barriers and are less efficient. RRKM calculations on the combined B3LYP and PMP2/6-311++G(2d,p) potential energy surface of the ground doublet electronic state of the peptide radicals provided rate constants that were quantitatively consistent with the dissociations observed in the gas phase. The formation of minor sequence z_1 and z_2 fragments from AHL was interpreted as occurring in the first excited state of the radical.

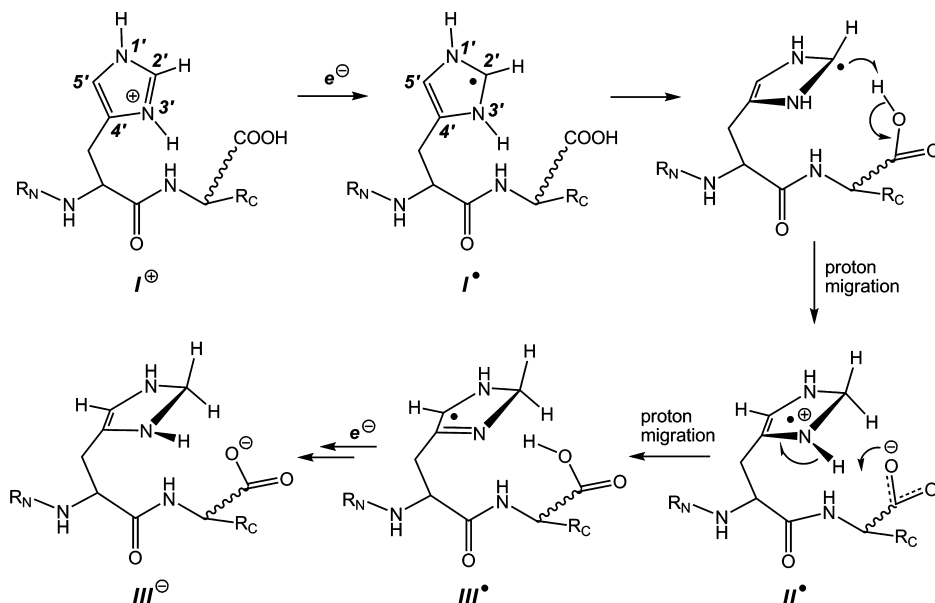
Introduction

Dissociations of gas-phase peptide ions are known to provide information on the peptide amino acid composition and sequence which are invaluable in protein identification using the bottom-up approach. The mechanistic aspects of peptide ion fragmentations have been studied in detail as reviewed.¹ A conspicuous feature of peptide ion dissociations is the presence of proton migrations that accompany or precede the formation of typical sequence fragments of the *b* and *y* type.² The energetics of peptide ion backbone fragmentations have been studied by experiment and theory and activation energies on the order of 100–150 kJ mol⁻¹ have been found to be typical.³ With the advent of electron-based methods, such as electron capture dissociation (ECD)⁴ and electron transfer dissociation in both

ion beams⁵ and ion traps,^{6,7} fundamental questions of dissociation mechanisms and energetics have been raised that need to be addressed. In particular, it has been recognized that the formation of sequence fragments of the *c* and *z* type, which are

- (1) (a) Laskin, J.; Furtell, J. H. *Mass Spectrom. Rev.* **2003**, *22*, 158–181.
(b) Paizs, B.; Suhai, S. *Mass Spectrom. Rev.* **2005**, *24*, 508–548.
- (2) (a) Roepstorff, P.; Fohlman, J. *Biomed. Mass Spectrom.* **1984**, *11*, 601. (b) Johnson, R. S.; Martin, S. A.; Biemann, K. *Int. J. Mass Spectrom. Ion Processes* **1988**, *86*, 137–154.

- (3) (a) Paizs, B.; Suhai, S. *J. Am. Soc. Mass Spectrom.* **2004**, *15*, 103–113. (b) Laskin, J.; Bailey, T. H.; Furtell, J. H. *Int. J. Mass Spectrom.* **2004**, *234*, 89–99. (c) Laskin, J.; Bailey, T. H.; Furtell, J. H. *Int. J. Mass Spectrom.* **2006**, *249*, 462–472. (d) Bythell, B. J.; Barofsky, D. F.; Pingitore, F.; Polce, M. J.; Wang, P.; Wesdemiotis, C.; Paizs, B. *J. Am. Soc. Mass Spectrom.* **2007**, *18*, 1291–1303. (e) Lioe, H.; Laskin, J.; Reid, G. E.; O'Hair, R. A. *J. Phys. Chem. A* **2007**, *111*, 10580–10588. (f) Cannon, W. R.; Taasevigen, D.; Baxter, D. J.; Laskin, J. *J. Am. Soc. Mass Spectrom.* **2007**, *18*, 1625–1637.
- (4) Zubarev, R. A.; Kelleher, N. L.; McLafferty, F. W. *J. Am. Chem. Soc.* **1998**, *120*, 3265–3266.
- (5) Boltalina, O. V.; Hvelplund, P.; Jørgensen, T. J. D.; Larsen, M. C.; Larsson, M. O.; Sharotchenko, D. A.; Sørensen, M. *Phys. Rev. A* **2000**, *62*, 023202.
- (6) Syka, J. E. P.; Coon, J. J.; Schroeder, M. J.; Shabanowitz, J.; Hunt, D. F. *Proc. Natl. Acad. Sci. U.S.A.* **2004**, *101*, 9528–9533.
- (7) Gunawardena, H. P.; He, M.; Chrisman, P. A.; Pitteri, S. J.; Hogan, J. M.; Hodges, B. D. M.; McLuckey, S. A. *J. Am. Chem. Soc.* **2005**, *127*, 12627–12639.

Scheme 1. Proton Migrations in Histidine Peptides Triggered by Electron Attachment

particular to electron-based dissociations, requires hydrogen migrations. McLafferty and co-workers suggested that the hydrogen migration originates in the charge-carrying functional group in the peptide ion that becomes a radical site upon electron attachment.⁸ This so-called Cornell mechanism⁹ involves aminoketyl radical intermediates. Analysis of the reaction energetics indicated that these have very low energy barriers to N-C_α bond cleavage¹⁰ and can account for dissociations of lysine containing peptide ions, as the lysine ammonium group becomes a good hydrogen atom donor upon electron attachment.¹¹ Depending on the peptide secondary structure, lysine ammonium hydrogens have been shown to undergo a virtually barrierless and highly exothermic migration onto sterically proximate carbonyl groups thus forming aminoketyl intermediates and triggering backbone fragmentation.¹¹ The hydrogen atom migration has been characterized as proton-coupled electron transfer¹² on the basis of orbital analysis and odd-electron density distribution in the reactants and transition states.¹¹ In contrast to lysine, the other two basic amino acids, arginine and histidine, have been shown to be inefficient hydrogen atom donors.^{13,14} Experiment and theory have shown that, both thermochemically and kinetically, the reduced guanidinium group in arginine residues is a poor hydrogen atom donor, while being a good acceptor of hydrogen atoms from sterically accessible α -positions along the peptide backbone.^{13b}

- (8) Zubarev, R. A.; Horn, D. M.; Fridriksson, E. K.; Kelleher, N. L.; Kruger, N. A.; Lewis, M. A.; Carpenter, B. K.; McLafferty, F. W. *Anal. Chem.* **2000**, *72*, 563–573.
- (9) Chen, X.; Tureček, F. *J. Am. Chem. Soc.* **2006**, *128*, 12520–12530.
- (10) Tureček, F. *J. Am. Chem. Soc.* **2003**, *125*, 5954–5963.
- (11) (a) Tureček, F.; Syrstad, E. A. *J. Am. Chem. Soc.* **2003**, *125*, 3353–3369. (b) Tureček, F.; Chen, X.; Hao, C. *J. Am. Chem. Soc.* **2008**, *130*, 8818–8833.
- (12) (a) Siegbahn, P. E. M.; Eriksson, L.; Himo, F.; Pavlov, M. *J. Phys. Chem. B* **1998**, *102*, 10622–10629. (b) Cuijier, R. I.; Nocera, D. G. *Annu. Rev. Phys. Chem.* **1998**, *49*, 337–369. (c) Mayer, J. M.; Hrovat, D. A.; Thomas, J. L.; Borden, W. T. *J. Am. Chem. Soc.* **2002**, *124*, 11142–11147.
- (13) (a) Hayakawa, S.; Matsubara, H.; Panja, S.; Hvelplund, P.; Nielsen, S. B.; Chen, X.; Tureček, F. *J. Am. Chem. Soc.* **2008**, *130*, 7645–7654. (b) Panja, S.; Nielsen, S. B.; Hvelplund, P.; Tureček, F. *J. Am. Soc. Mass Spectrom.* **2008**, *19*, 1726–1742.
- (14) Tureček, F.; Jones, J. W.; Towle, T.; Panja, S.; Nielsen, S. B.; Hvelplund, P.; Paizs, B. *J. Am. Chem. Soc.* **2008**, *130*, 14584–14596.

Recently, McLuckey and co-workers reported an electron transfer dissociation study of histidine-containing peptide ions that were found to resist fragmentation upon electron transfer from azobenzene anion radicals.¹⁵ Since these early reports, several other histidine-containing peptide ions have been found to produce stable radicals or cation-radicals upon femtosecond electron transfer from gaseous Cs atoms, indicating that this behavior is of a general nature. The unusual stability of His containing peptide radicals has been explained by rearrangements in the charge-reduced intermediates, which underwent reverse hydrogen migrations onto the His imidazole ring.¹⁴ It has been suggested that the rearrangement produces stable imidazoline radical intermediates that were detected as charge-reduced cations or anions after collisional reionization. The basic mechanistic aspects of the histidine rearrangement have been outlined for model dipeptides Gly-His and His-Gly¹⁶ and tripeptide His-Ala-Ile.¹⁴ This type of rearrangement in a peptide ion (I^+) requires an interaction between the C-2' position in the histidine imidazolium radical produced by electron attachment (I^{\bullet}) and a sterically proximate carboxyl group (Scheme 1). Calculations on the electronic structure of these model systems indicated that the rearrangement was exothermic and proceeded with an extremely low activation energy. An unusual feature of this reaction is that it proceeds as a carboxyl proton transfer to the imidazolium radical forming a zwitterionic intermediate (II^*). The latter is stabilized by a strong Coulomb interaction between the charges on the separated imidazolium cation-radical and carboxylate anion (Scheme 1). In the absence of the stabilizing Coulomb interaction, the rearrangement was calculated to be endothermic. The zwitterionic intermediate II^* may undergo further exothermic proton migration forming imidazoline radical III^{\bullet} , which is detected as such if it carries an additional charge, or as a stable anion (III^-) upon second electron transfer. The stabilizing Coulomb interaction in II^* as well as the proton migrations strongly depend on the spatial

- (15) Xia, Y.; Gunawardena, H. P.; Erickson, D. E.; McLuckey, S. A. *J. Am. Chem. Soc.* **2007**, *129*, 12232–12243.
- (16) Tureček, F.; Yao, C.; Fung, Y. M. E.; Hayakawa, S.; Hashimoto, M.; Matsubara, H. *J. Phys. Chem. B* **2009**, *113*, 7347–7366.

arrangement of the charged groups and thus can be expected to be sensitive to the peptide amino acid sequence and secondary structure.

We now address this novel peptide chemistry in a joint experimental and computational study with a series of tripeptides that differ in their amino acid sequence, presence or absence of free carboxyl group, and the steric accessibility of the imidazole ring in the histidine side chain. Singly protonated tripeptides HAL, AHL, ALH, and HAL-amide were studied by charge-reversal ($^{+}\text{CR}^-$) mass spectrometry and combined molecular dynamics/density functional theory/Møller-Plesset theory calculations in an effort to elucidate reactive and stable intermediates formed by electron transfer in the gas phase. These peptide sequences were selected to alter interactions between the histidine ring and the carboxylate group in HAL, AHL, and ALH, and prevent them completely in HAL-NH₂. The unique feature of the charge-reversal approach is that only radicals having positive electron affinities can form stable anions. In contrast, N-3'-H imidazolium radicals of the type **I'** (Scheme 1) do not have bound anionic states.¹⁴ Thus, detection of a stable peptide anion provides unequivocal evidence for a rearrangement in the peptide radicals. Another feature of $^{+}\text{CR}^-$ experiments, which is favorable for fundamental studies, is that they allow one to generate and study radical intermediates from singly charged precursor ions. Thus, the experiments are not limited by insufficient peptide charging upon ionization which is a well recognized problem in ETD.⁶ Furthermore, $^{+}\text{CR}^-$ experiments with Cs probe radical intermediates on a 10⁻⁷ s time scale, which is at least 5 orders of magnitude shorter than in studies using electron capture or transfer in ion traps. Hence, much faster processes can be studied than those addressed by ECD/ETD. By probing structures of short-lived intermediates we gain insight into processes occurring shortly after the electron transfer, while mostly avoiding complications caused by ion-molecule reactions occurring in ECD/ETD when performed in ion traps.¹⁷ The use of Cs as an electron donor benefits from good collisional cross sections for electron transfer from alkali metal atoms,¹⁸ the very low ionization energy of atomic Cs (3.894 eV), and high excitation energies of Cs⁺ ions.

Experimental Section

Materials and Methods. The tripeptides, HAL, AHL, ALH, and HAL amide (>95% purity) were purchased from GenScript (Piscataway, NJ). The peptides were characterized by electrospray (ESI) mass spectra in combination with collision induced dissociation (CID) of the respective (M + H)⁺ ions (MS/MS) to verify the amino acid sequence. The CID spectra of HAL and AHL are given in Figure S1a,b (Supporting Information). CID and charge inversion ($^{+}\text{CR}^-$) mass spectra were measured on a large-scale sector instrument described previously.¹⁹ Briefly, the instrument consists of an electrospray ionization source and a three-stage pumping

system that are mounted on a high-voltage platform floated at 50 kV. Ions produced in the source are accelerated to 50 keV (z = ion charge) and separated by a double-focusing magnetic sector of a 2 m radius and 72° deflection angle. The magnetic sector achieves a $M/\Delta M$ dispersion of 1364 in the focal plane at the mass-resolving slit. Mass-selected ions enter a special differentially pumped collision cell that contains a resistively heated reservoir of Cs. The partial pressure of Cs vapor is controlled by adjusting the reservoir temperature. Products of ion–Cs collisions pass a variable-width energy-resolving slit and travel to a 180° electrostatic analyzer (ESA) that is located 80 cm after the collision cell. Energy-resolved ions are detected by a counting electron multiplier (Ceratron-E, Murata, Japan), the counts are filtered by an Ortec timing-filter amplifier and processed by a home-built data acquisition system. Singly protonated ions were produced by electrospray ionization from 1:1 water/methanol solutions containing 1% of acetic acid. Precursor (M + H)⁺ ions were accelerated to 50 keV corresponding to velocities of 1.68×10^5 m s⁻¹. The ions were mass-selected by a magnetic sector at mass resolution >1000 and subjected to collisions with Cs vapor in a special cell. The ion drift time through the 4 cm long collision cell was $t = 240$ ns for the fast peptide ions under study, during which time the ions underwent two collisions with Cs atoms. Radicals formed by the first collision have a Poisson distribution of drift times prior to being ionized by a second collision. The distribution peaks at $t/2 = 120$ ns, which represents the most probable radical lifetime.²⁰ The temperature in the cell was maintained at 105 °C corresponding to about 40–50% precursor ion beam transmittance. Negative ions formed in the cell were separated by kinetic energy and detected by ion counting. Multiple scans were taken and averaged to obtain sufficient ion counts for most negative ions. Spectra of (M + H)⁻ anions from AHL were also measured with a narrow (0.1 mm) ESA entrance slit for increased kinetic energy and mass resolution.

Calculations. Our conformational search of the potential energy surface (PES) of the peptide ions employed a search engine specially devised to deal with protonated peptides.²¹ These calculations started with molecular dynamics (MD) simulations on the N-terminal amino and His side-chain protonated tautomers using the Insight II program (Biosym Technologies, San Diego, CA) in conjunction with a modified AMBER force field.²² During the MD we used simulated annealing techniques to produce candidate structures for further refinement, applying full geometry optimization using the modified AMBER force field. The AMBER optimized structures were analyzed by a conformer family search program developed in Heidelberg.^{21b} This program groups optimized structures into families for which the most important characteristic torsion angles of the molecule were similar. The most stable species in the families were then fully optimized with PM3 and ranked by energy by HF/3-21G single-point energy calculations. The 40 lowest-energy conformers from the above-described search in each group of protonation tautomers were then reoptimized with density functional theory calculations²³ using B3LYP/6-31+G(d,p) and including harmonic frequency analysis. These calculations were performed using the Gaussian 03 suite of programs.²⁴ Enthalpies and entropies were calculated using the rigid-rotor-harmonic oscillator (RRHO) approximation. Although absolute enthalpies and entropies are likely to be exaggerated by RRHO due to the presence

- (17) (a) Lin, C.; O'Connor, P. B.; Cournoyer, J. J. *J. Am. Soc. Mass Spectrom.* **2006**, *17*, 1605–1615. (b) O'Connor, P. B.; Lin, C.; Cournoyer, J. J.; Pittman, J. L.; Belyayev, M.; Budnik, B. A. *J. Am. Soc. Mass Spectrom.* **2006**, *17*, 576–585. (c) Savitski, M. M.; Kjeldsen, F.; Nielsen, M. L.; Zubarev, R. A. *J. Am. Soc. Mass Spectrom.* **2007**, *18*, 113–120.
- (18) (a) Williams, B. W.; Porter, R. F. *J. Chem. Phys.* **1980**, *73*, 5598–5604. (b) Gellene, G. I.; Porter, R. F. *Acc. Chem. Res.* **1983**, *16*, 200–207. (c) Blanchette, M. C.; Bordas-Nagy, J.; Holmes, J. L.; Hop, C. E. C. A.; Mommers, A. A.; Terlouw, J. K. *Org. Mass Spectrom.* **1988**, *23*, 804–807. (d) Wesdemiotis, C.; Feng, R. *Org. Mass Spectrom.* **1988**, *23*, 416–418. (e) McLafferty, F. W.; Wesdemiotis, C. *Org. Mass Spectrom.* **1989**, *24*, 663–668.
- (19) Larsson, M. O.; Hvelplund, P.; Larsen, M. C.; Shen, H.; Cederquist, H.; Schmidt, H. T. *Int. J. Mass Spectrom.* **1998**, *177*, 51–62.
- (20) Hayakawa, S.; Matsubara, H.; Panja, S.; Hvelplund, P.; Nielsen, S. B.; Chen, X.; Tureček, F. *J. Am. Chem. Soc.* **2008**, *130*, 7645–7654.
- (21) (a) Wytenbach, T.; Paizs, B.; Barran, P.; Breci, L. A.; Liu, D.; Suhai, S.; Wysocki, V. H.; Bowers, M. T. *J. Am. Chem. Soc.* **2003**, *123*, 13768–13775. (b) Paizs, B.; Suhai, S.; Hargittai, B.; Hruby, V. J.; Somogyi, A. *Int. J. Mass Spectrom.* **2002**, *219*, 203–232.
- (22) Case, D. A., *AMBER 99*; University of California: San Francisco, 1999.
- (23) (a) Becke, A. D. *J. Chem. Phys.* **1993**, *98*, 1372–1377. (b) Becke, A. D. *J. Chem. Phys.* **1993**, *98*, 5648–5652. (c) Stephens, P. J.; Devlin, F. J.; Chabalowski, C. F.; Frisch, M. J. *J. Phys. Chem.* **1994**, *98*, 11623–11627.
- (24) Frisch, M. J., *Gaussian 03, Revision E.01*; Gaussian, Inc.: Pittsburgh PA, 2003.

in the ions of multiple low-frequency modes, relative enthalpies and entropies were deemed to be reliable due to cancellation of errors. The fully optimized ion structures were sorted out by their relative enthalpies and free energies. A total of 24 structures of the lowest free-energy group were submitted to single-point energy calculations using B3LYP and MP2 (frozen core)²⁵ with the larger 6-311++G(2d,p) basis set of triple- ζ quality furnished with polarization and diffuse functions on all atoms. Tables S1–S60 of complete optimized structures are available as Supporting Information.

Radical structures were optimized with B3LYP/6-31++G(d,p) using the spin unrestricted formalism. Local energy minima and transition states were characterized by harmonic frequency analysis to have the appropriate number of imaginary frequencies (zero for local minima and one for transition states). Additional sets of energies were obtained by single-point calculations on the B3LYP-optimized geometries. The single-point calculations used B3LYP and Møller–Plesset perturbational theory²⁵ truncated at second order with valence electrons only excitations (MP2 (frozen core)) and the 6-311++G(2d,p) basis set. For molecular systems of the (HAL + H)[·] radical size the larger basis set comprised 1242 primitive gaussians. The spin unrestricted formalism was used for calculations of open-shell systems. Contamination by higher spin states was modest, as judged from the expectation values of the spin operator $\langle S^2 \rangle$ that were ≤ 0.76 for UB3LYP and ≤ 0.78 for UMP2 calculations for most radicals. The UMP2 energies were corrected by spin annihilation²⁶ that reduced the $\langle S^2 \rangle$ to close to the theoretical value for a pure doublet state (0.75). The single point B3LYP and spin-projected MP2 energies were averaged (B3-PMP2),²⁷ which resulted in cancellation of small errors in the relative energies inherent to both approximations and provided dissociation and transition state energies of improved accuracy, as has been previously shown for a number of closed-shell and open-shell systems. The B3-PMP2 correction scheme is supported by the analysis of bond dissociation in H₂, where B3LYP was found to overestimate the correlation energy, while MP2 underestimated it by the same amount when compared to full-CI reference calculations.²⁸ Single-point energies for model imidazole ions, radicals, and transition states were also obtained by benchmark coupled-cluster calculations, as reported previously.¹⁴ Atomic spin and charge densities were calculated using the natural population analysis (NPA) method.²⁹ The electronic excitation energies were calculated using time-dependent density functional theory³⁰ using B3LYP/6-311++G(2d,p). Unimolecular rate constants were calculated using the Rice–Ramsperger–Kassel–Marcus (RRKM) theory³¹ and employing Hase's program,³² which was recompiled for Windows XP. The RRKM rate constants were obtained by direct count of quantum states at internal energies that were increased in 2 kJ mol⁻¹ steps from the transition state up to 400 kJ mol⁻¹ above the reactant. We treated the rotations adiabatically and calculated

- (25) Møller, C.; Plesset, M. S. *Phys. Rev.* **1934**, *46*, 618–622.
- (26) (a) Schlegel, H. B. *J. Chem. Phys.* **1986**, *84*, 4530–4534. (b) Mayer, I. *Adv. Quantum Chem.* **1980**, *12*, 189–262.
- (27) Tureček, F. *J. Phys. Chem. A* **1998**, *102*, 4703–4713.
- (28) Rassolov, V. A.; Ratner, M. A.; Pople, J. A. *J. Chem. Phys.* **2000**, *112*, 4014–4019.
- (29) Reed, A. E.; Weinstock, R. B.; Weinhold, F. *J. Chem. Phys.* **1985**, *83*, 735–746.
- (30) Stratmann, R. E.; Scuseria, G. E.; Frisch, M. J. *J. Chem. Phys.* **1998**, *109*, 8218–8224.
- (31) Gilbert, R. G.; Smith, S. C. *Theory of Unimolecular and Recombination Reactions*; Blackwell Scientific Publications: Oxford, 1990; pp 52–132.
- (32) Zhu, L.; Hase, W. L. *Quantum Chemistry Program Exchange*; Indiana University: Bloomington, 1994; Program No. QCPE 644.

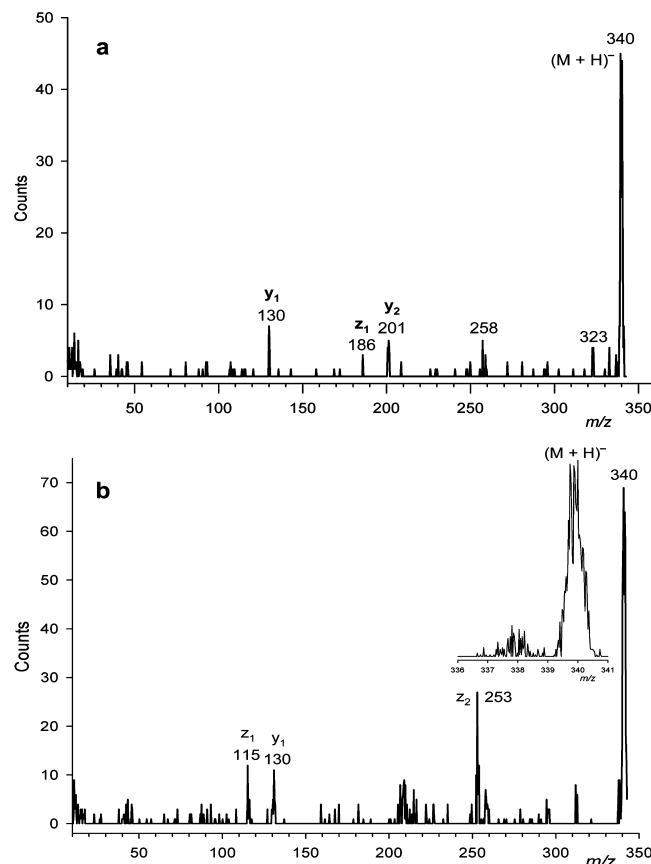


Figure 1. ${}^{+}\text{CR}^{-}$ mass spectra of (a) (HAL + H)⁺ and (b) (AHL + H)⁺. Inset shows the m/z 336–341 region with the nondissociated molecular anion of (AHL + H)⁻.

the microscopic rate constants $k(E,J,K)$, which were then Boltzmann-averaged over the thermal distribution of rotational states at 298 K.

Results

Charge-Reversal Mass Spectra. Charge reversal from cations to anions is a two-collision process³³ in which precursor peptide cations are converted to radicals in the first collision and a fraction of peptide radicals and their neutral dissociation products are converted to anions in a second collision with Cs atoms. Concomitant with collisional electron transfer, collisional activation of precursor cations induces dissociations forming neutral fragments that can be ionized by electron attachment and appear as anions in the ${}^{+}\text{CR}^{-}$ spectra.³⁴

The ${}^{+}\text{CR}^{-}$ mass spectra of protonated HAL and AHL show dominant peaks at m/z 340 which correspond to undissociated anions, (HAL + H)⁻ and (AHL + H)⁻, respectively, or their isomers (Figure 1a,b). The intensities of these survivor anions, relative to the sum of all anion peaks in the ${}^{+}\text{CR}^{-}$ spectra, are practically the same for HAL and AHL, for example, 46 \pm 3%.³⁵ Fragmentations resulting from double collisions include

- (33) (a) Schroder, D. Charge Reversal. In *The Encyclopedia of Mass Spectrometry*; Armentrout, P. B., Ed.; Elsevier: Amsterdam, 2003; Vol. 1, Chapter 8, pp 521–528. (b) Hayakawa, S. *J. Mass Spectrom.* **2004**, *39*, 111–135.
- (34) Hvelplund, P.; Liu, B.; Nielsen, S. B.; Panja, S.; Pouilly, J.-C.; Stöckkel, K. *Int. J. Mass Spectrom.* **2007**, *263*, 66–70.
- (35) The uncertainties are one standard deviation from Poisson ion counting statistics. ${}^{+}\text{CR}^{-}$ mass spectra of (HAL + H)⁺ ions measured one year apart showed 46–48% of nondissociated anions.

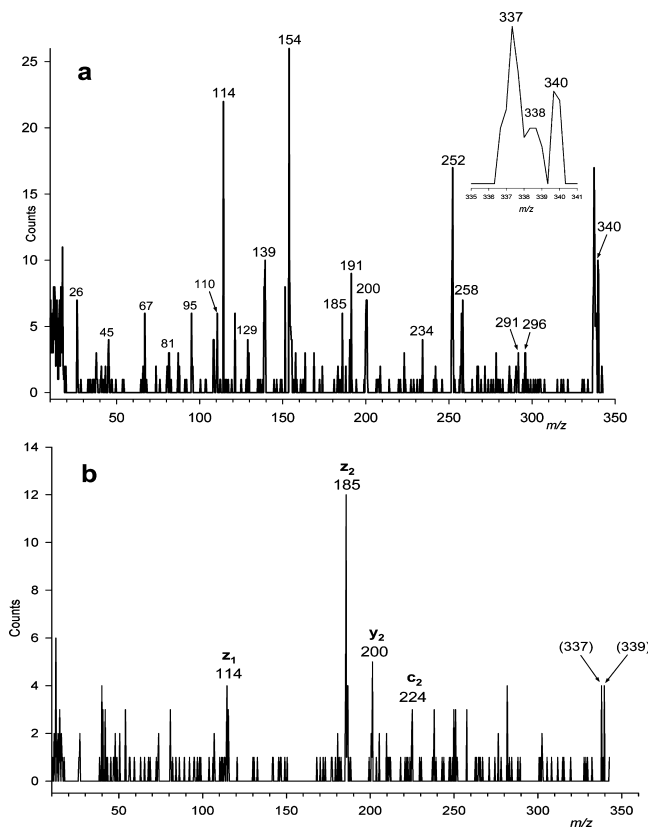


Figure 2. ${}^+\text{CR}^-$ mass spectra of (a) $(\text{ALH} + \text{H})^+$ and (b) $(\text{HAL}-\text{NH}_2 + \text{H})^+$. Inset shows the m/z 335–341 region with the nondissociated molecular anion of $(\text{ALH} + \text{H})^-$.

loss of two hydrogen atoms (m/z 338, Figure 1b, inset), ammonia (m/z 323), histidine side chain (m/z 258), and backbone cleavages giving sequence fragments. For HAL, the latter are observed at m/z 201 (y_2^-), 186 (z_2^-), 130 (y_1^-), and 115 (z_1^-). For AHL, sequence fragments are observed at m/z 253 (z_2^-), 209 (b_2^-), 130 (y_1^-), and 115 (z_1^-). Note that the y^- fragments correspond to deprotonated AL or leucine, whereas the z^- fragments correspond to z radicals with an attached electron.² The y_1^- ions in the ${}^+\text{CR}^-$ spectra may also arise by dissociative electron transfer to Leu molecules, which are the neutral counterparts of major b_2 ions from ion dissociations, as established from CID spectra (Figure S1, Supporting Information). In contrast, the z anions in the ${}^+\text{CR}^-$ spectra do not have abundant counterparts in the CID spectra and must arise by radical or anion dissociations triggered by electron transfer.

The ${}^+\text{CR}^-$ mass spectra of protonated ALH and HAL amide dramatically differ from those of HAL and AHL. The ${}^+\text{CR}^-$ spectrum of ALH (Figure 2a) shows a peak of undissociated anion $(\text{ALH} + \text{H})^-$ albeit at much lower relative intensity ($4 \pm 1\%$) than those from HAL and AHL. Fragments are observed at m/z 338, 337 (loss of 2H and 3H), 258 (loss of His side chain), 252 (z_2^-), 154 (y_1^-), 139 (z_1^-), and 114. The latter is presumably an internal Leu fragment ($\text{C}_6\text{H}_{12}\text{NO}$).

The ${}^+\text{CR}^-$ spectrum of HAL amide was very difficult to obtain because of an extremely poor cation to anion conversion. The spectrum shown in Figure 2b was obtained after >20 h of data acquisition and consists of 256 anion counts from about 5×10^9 precursor cations that were subjected to collisional electron transfer. The spectrum shows sequence z_1^- (m/z 114),

z_2^- (m/z 185), and y_2^- (m/z 200) ions and a few other minor fragments including four ion counts for the survivor anion at m/z 339.

In summary, the presence of an abundant survivor anion peptide peak in the ${}^+\text{CR}^-$ spectra appears to critically depend on both the position of the His residue in the amino acid sequence and the presence of a free carboxyl group. These effects must be linked to the structure of intermediate peptide radicals formed by electron transfer and their propensity to accommodate an additional electron upon collisional transfer from Cs to form stable anions. To interpret these effects we carried out a detailed analysis of several pertinent cations, radicals, and anions using electron structure theory, as described in the next section.

Precursor Ion Structures. Analysis of the conformational space for HAL, AHL, ALH, and HAL amide provided several groups of conformers for ion tautomers protonated in the His imidazole ring and at the N-terminal amino group. In all cases, the His-protonated tautomers were substantially more stable than the N-terminally protonated ones. Five groups of His-protonated HAL conformers (**h1⁺–h5⁺**) were identified as the lowest energy structures by combined B3LYP and MP2 calculations (Figure 3, Table 1). Groups **h1⁺–h5⁺** each consisted of multiple rotamers that shared the same hydrogen bonding pattern but differed in side chain conformations. The lowest energy rotamers in each group are shown in Figure 3. Ions **h1⁺–h5⁺** all have strong hydrogen bonds between the N-3'-H proton of the His ring and the Ala amide oxygen. The conformers differ in the pattern of hydrogen bonds between the neutral polar groups. According to the calculated free energies (Table 1), the equilibrium populations of rotamers of the **h1⁺**, **h2⁺**, and **h3⁺** groups were 70, 16, and 12%, respectively, at 298 K. The other conformers (**h4⁺**, **h5⁺**) and the N-terminus protonated species **h6⁺** and **h7⁺** had higher free energies and presumably were much less populated and so they represent only minor components of the ion conformer mixture in the gas phase. Table 1 shows that B3LYP and MP2 calculations gave similar rankings for the ion conformers and tautomers. Ion **h4⁺** was an exception in that MP2 ranked it as the thermochemically most stable structure. In view of this minor discrepancy, all five low-energy ions **h1⁺–h5⁺** were considered as precursors for the formation of radicals by electron attachment.

The protonated HAL amides were found to have protonation sites and conformations analogous to the HAL peptide ions. The most stable conformers are shown in Figure S2 (Supporting Information).

The conformational space of protonated AHL peptides showed five groups of His-protonated structures which are represented by the lowest energy conformer in each group (**a1⁺–a5⁺**, Figure 4). It is worth noting that B3LYP/6-311++G(2d,p) calculations favored the **a1⁺** group as the global minimum, whereas MP2/6-311++G(2d,p) calculations preferred the **a2⁺** group of rotamers. Likewise, B3LYP ranked the N-terminus protonated tautomer (**a6⁺**) as being a high-energy species (Table 2), whereas MP2 placed ion **a6⁺** as the second ranking isomer after **a2⁺**. Structures **a2⁺** and **a6⁺** are remarkably similar (Figure 4), differing only in the position of the proton, which is chelated between the N-terminal amino group and the N-3' histidine position. The reason for the preference by MP2 for structures **a2⁺** and **a6⁺** is not clear but may be due to the presence of strong N...H...N hydrogen bonds in both tautomers. We note that discrepancies between B3LYP and MP2 calculations in assigning structures have been reported recently

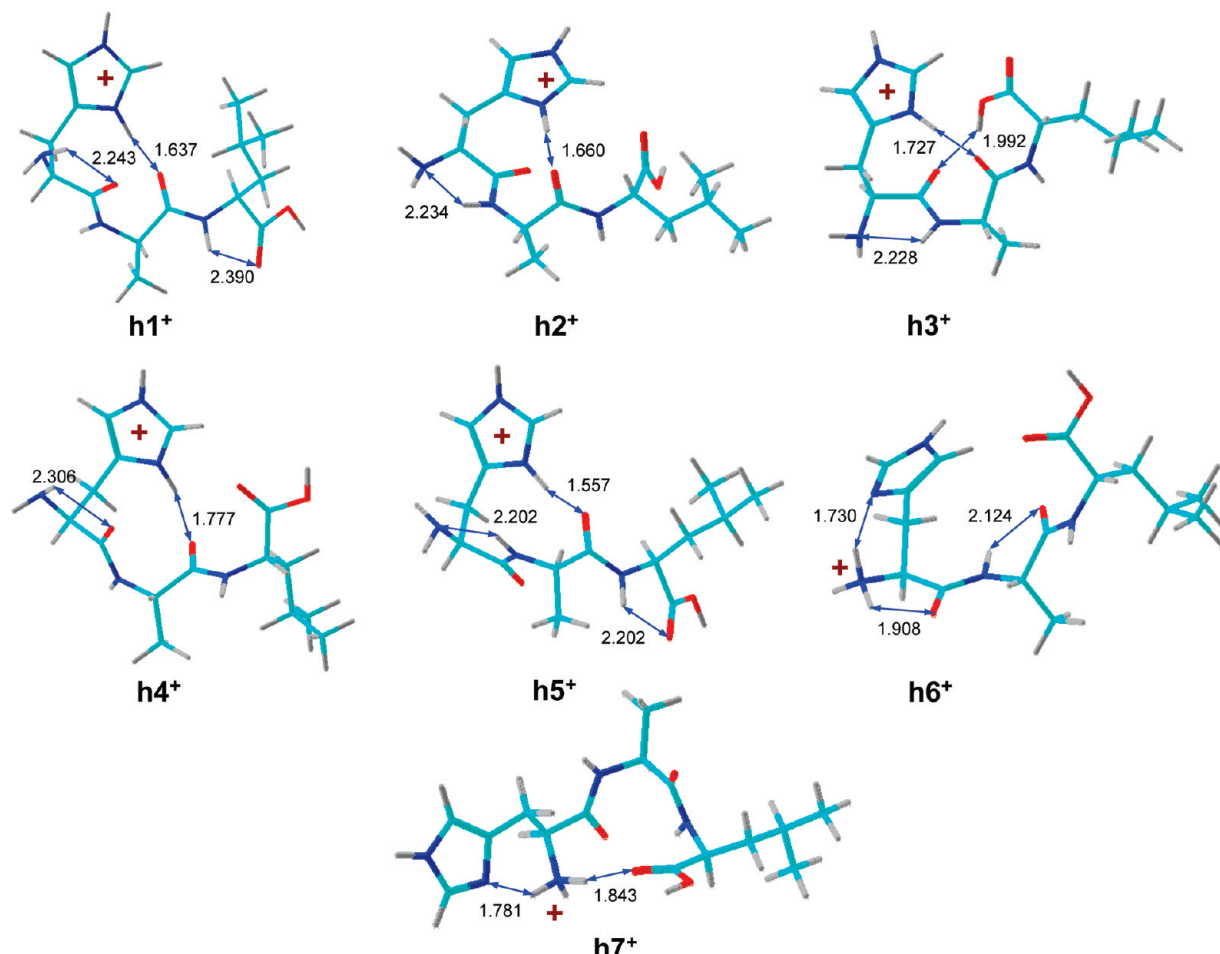


Figure 3. B3LYP/6-31+G(d,p) optimized structures of (HAL + H)⁺ ions. Hydrogen bonds are denoted by blue double arrows. Atoms are color-coded as follows: turquoise, C; blue, N; red, O; gray, H.

Table 1. Relative Energies of Protonated HAL Peptides

ion	relative energy ^{a,b}			
	B3LYP		MP2	B3-MP2
	6-31+G(d,p)	6-311++G(2d,p)	6-311++G(2d,p)	6-311++G(2d,p)
h1⁺	4.2	2.0	5.9	4.0 (−4.6)
h2⁺	0.0	0.0	0.0	0.0 (0.0) ^c
h3⁺	8.1	6.8	4.7	5.7 (0.3)
h4⁺	9.0	8.5	−1.3	3.6 (7.1)
h5⁺	8.1	7.5	12	9.8 (4.5)
h6⁺	23	22	14	18 (14)
h7⁺	21	22	21	22 (19)

^a In units of kJ mol^{−1}. ^b Including B3LYP/6-31+G(d,p) zero-point vibrational energies and referring to 0 K unless stated otherwise.

^c Values in parentheses are relative free energies at 298 K.

for other gas-phase peptide ions.³⁶ Because of the tight hydrogen bonding, ion **a2⁺** is less entropically favored than **a1⁺** and **a3⁺**, so that structures **a1⁺–a3⁺** are practically indistinguishable by free energy at the present level of theory. Because of the ambiguity in assigning the most stable conformer for AHL ions, we considered the three most stable His-protonated tautomers and the N-terminally protonated one as plausible precursors for the formation of radicals by electron transfer.

The ALH peptides showed a definite preference for structures protonated in the His imidazole ring (**x1⁺–x4⁺**, Figure 5). The

most stable N-terminally protonated tautomers (**x5⁺, x6⁺**, Figure 5) had substantially higher energies by both B3LYP and MP2 (Table 3) and were unlikely to be significantly populated at 298 K. Again, the calculated single-point energies did not allow us to assign the most stable conformer among the His-protonated structures, as B3LYP slightly preferred structure **x1⁺** and while MP2 slightly preferred structure **x2⁺**. In view of the very small differences in the conformer energies, we considered all four lowest energy conformers (**x1⁺–x4⁺**) as possible precursors for radicals in the ALH group.

Peptide Radicals

Recombination Energies. Due to the nature of the charge-transfer experiments, collisional electron transfer from the Cs atom to the fast moving ion is confined to occur within 6–9 fs when the precursor ion and the cesium atom are within a 10–15 Å distance, corresponding to the collisional cross section. This time is shorter than the vibrational periods of all nuclear motions in the ion and thus the electron transfer can be considered a vertical transition and characterized by a vertical recombination energy (RE_v). Following electron transfer, the radical intermediates exist for 120–240 ns before the second electron transfer occurs, and this time is considered sufficient for geometry relaxation and vibrational energy redistribution to reach the local potential energy minimum. The vibrational excitation in thus formed radicals, that is, the Franck–Condon energy (E_{FC}), is approximated by the difference between the adiabatic and

(36) (a) Wu, R.; McMahon, T. B. *J. Am. Chem. Soc.* **2007**, *129*, 11312–11313. (b) Wu, R.; McMahon, T. B. *J. Phys. Chem. B* **2009**, *113*, 8767–8775.

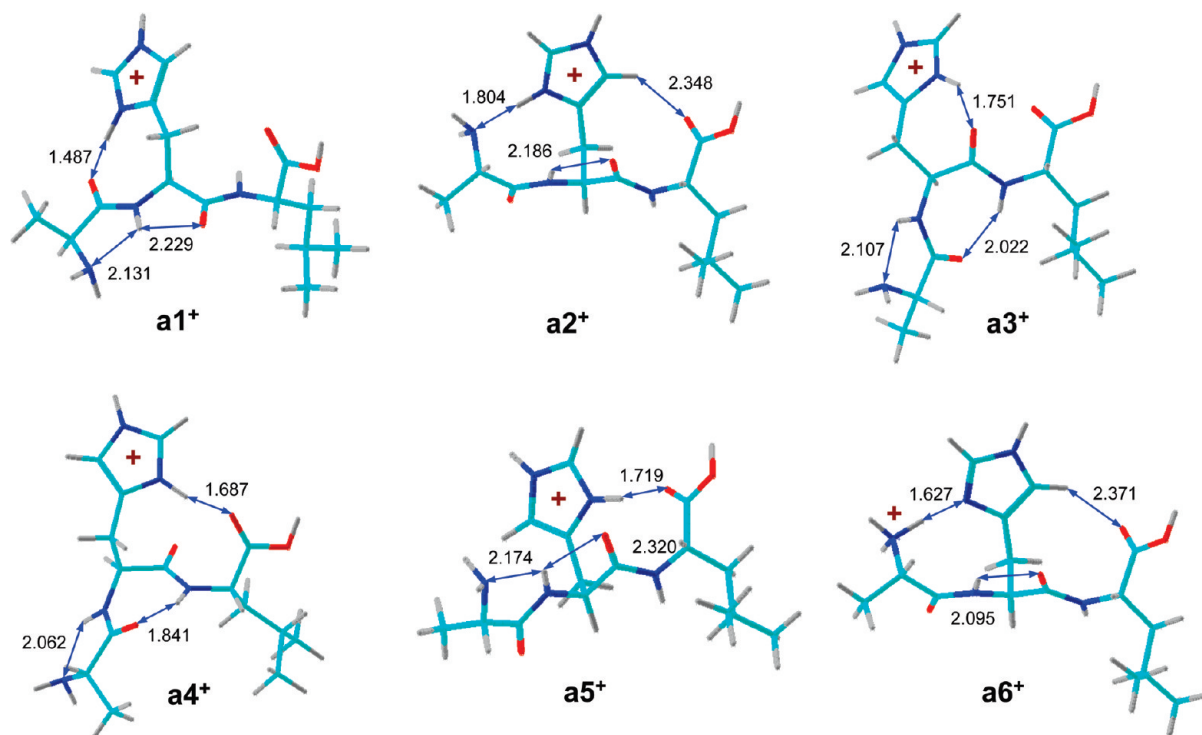


Figure 4. B3LYP/6-31+G(d,p) optimized structures of $(\text{AHL} + \text{H})^+$ ions. Atom color-coding and hydrogen bonds as in Figure 3.

Table 2. Relative Energies of Protonated AHL Peptides

ion	relative energy ^{a,b}			
	B3LYP	B3LYP	MP2	B3-MP2
	6-31+G(d,p)	6-311++G(2d,p)	6-311++G(2d,p)	6-311++G(2d,p)
a1⁺	0.0	0.0	0.0	0.0 (0.0) ^c
a2⁺	3.3	4.9	-14	-4.6 (0.3)
a3⁺	3.5	4.3	-5.3	-0.5 (0.1)
a4⁺	14	15	4.9	10 (15)
a5⁺	12	12	2.5	7.3 (6.4)
a6⁺	17	18	-9	4.0 (10)

^a In units of kJ mol^{-1} . ^b Including B3LYP/6-31+G(d,p) zero-point vibrational energies and referring to 0 K unless stated otherwise.

^c Values in parentheses are relative free energies at 298 K.

vertical recombination energies, $E_{\text{FC}} = |\text{RE}_a - \text{RE}_v|$. The values of RE_a and RE_v are summarized in Table 4. The adiabatic recombination energies for all His-protonated peptide ions studied here fell within 3.2–3.5 eV and were lower than the ionization energy of atomic Cs (3.894 eV).³⁷ In addition, the peptide ions exhibited substantial Franck–Condon energies (E_{FC}) upon vertical electron transfer, which ranged between 71–88 kJ mol^{-1} and contributed to vibrational excitation in the radicals. This excitation was mainly due to a mismatch of the relaxed geometries of the protonated His ring in the cations and radicals, as discussed previously.^{14,16} The N-terminally protonated AHL ion **a6⁺** had the lowest adiabatic recombination energy of the present set (2.89 eV) and relatively low E_{FC} (20 kJ mol^{-1}). This is consistent with the formation of a hypervalent ammonium radical (**a6**) in the ground electronic state.³⁸

The fact that electron transfer from Cs is endothermic requires that a small part of the nonfixed collision energy ($0.281 \times T_{\text{kin}}$

= 14 keV) be converted to internal energy to make up for the reaction endothermicity. It has been shown that under such conditions of endothermic electron transfer, the internal energy distribution in the radicals is a convolution of the internal energy distribution in the precursor ion and the distribution of the Franck–Condon energies for each electronic state of the radical.³⁹ The mean value can be approximated by a sum of the precursor ion ro-vibrational enthalpy (H_{ion}) and the Franck–Condon energy (E_{FC}). The tripeptide ions under study formed by electrospray have 298 K ro-vibrational enthalpies of 53–54 kJ mol^{-1} that, when combined with the Franck–Condon energies, give the mean internal energies in the radicals to be in the range of 124–142 kJ mol^{-1} .

HAL Radical Structures and Isomerizations. Electron transfer to HAL ions **h1⁺–h4⁺** followed by geometry relaxation gave radicals **h1–h4** as local energy minima. The main differences between the ion and radical geometries are (1) longer N–C bonds in the His ring, (2) ring puckering, and (3) weakened hydrogen bonding in the radicals. Radical **h1** corresponding to the most stable ion **h1⁺** showed an initial conformation that resembled that of the precursor ion. In contrast, radicals **h2–h4** each underwent a conformational transformation upon geometry optimization yielding new structures in which the proton of the COOH group was hydrogen-bonded to the C-2' position of the His ring (Scheme 2). This hydrogen bonding is facilitated by the electron density distribution within the radical N-1'-H imidazole ring where C-2' carries 50% of the unpaired electron density. Radicals **h3** and **h4** showed quite analogous electron density distribution and interactions with the COOH group as did **h2**, and their structures are shown in Scheme S1 (Supporting Information). The relative energies for HAL radicals are collated in Table 5.

The structures of **h2–h4** are prone for facile migration of the carboxyl proton onto C-2'. The pertinent transition state

(37) Lide, D. R., Ed.; *CRC Handbook of Chemistry and Physics*, 88th ed.; CRC Press: Boca Raton, FL, 2007–2008; Vols. 10–157, pp 10–202.

(38) Yao, C.; Tureček, F. *Phys. Chem. Chem. Phys.* **2005**, 7, 912–920.

(39) Tureček, F. *Int. J. Mass Spectrom.* **2003**, 227, 327–338.

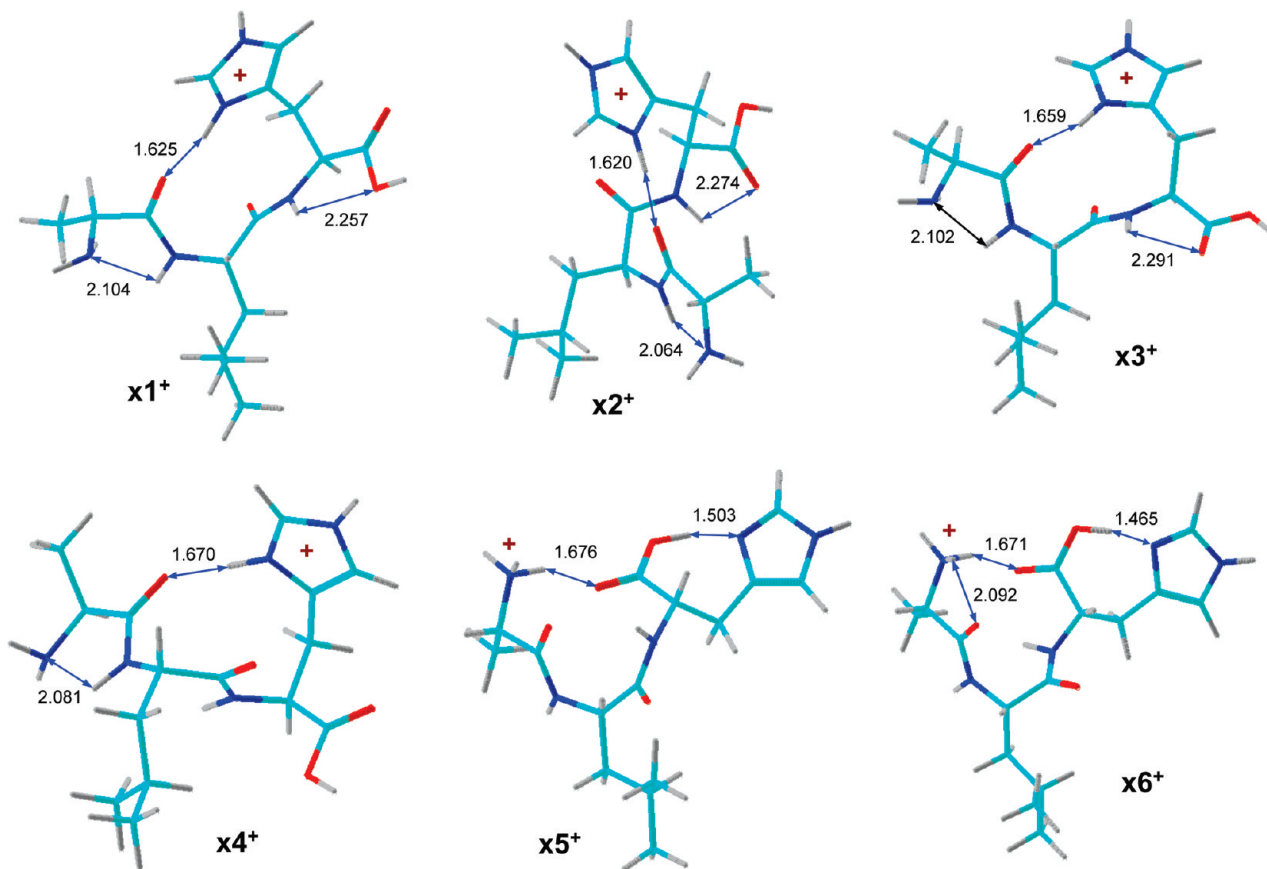


Figure 5. B3LYP/6-31+G(d,p) optimized structures of $(\text{ALH} + \text{H})^+$ ions. Atom color-coding and hydrogen bonds as in Figure 3.

Table 3. Relative Energies of Protonated ALH Peptides

ion	relative energy ^{a,b}			
	B3LYP		B3-MP2	6-311++G(2d,p)
	6-31+G(d,p)	6-311++G(2d,p)	MP2	
x1⁺	0.0	0.0	0.0	0.0 (0.0) ^c
x2⁺	3.2	3.4	-2.2	0.6 (1.9)
x3⁺	3.1	2.1	4.5	3.3 (2.5)
x4⁺	15	16	-0.8	7.6 (15)
x5⁺	25	26	19	23 (22)
x6⁺	27	27	23	25 (24)

^a In units of kJ mol^{-1} . ^b Including B3LYP/6-31+G(d,p) zero-point vibrational energies and referring to 0 K unless stated otherwise.

^c Values in parentheses are relative free energies at 298 K.

(TS1) for **h2** is shown in Scheme 2; those for **h3** and **h4** were quite analogous (Scheme S1) and need not be discussed separately. Instead of reaching **TS1**, radical **h2** can undergo a rotation of the COOH group to produce rotamer **h2a** which was 13 kJ mol^{-1} more stable than **h2** (Table 5). Rotamer **h2a** retains the $\text{COOH}\cdots\text{C-2}'$ interaction and can readily rearrange by proton migration through **TS2**. The products of H migration in **h2** and **h2a** differ depending on the orientation of the COOH group. Hydrogen migration through **TS1** forms intermediate **h2b**, which can be characterized as an unusual zwitterion consisting of an imidazoline cation-radical and a carboxylate anion. Indeed, the calculated atomic charges and spin densities from Natural Population Analysis (NPA) indicate substantial positive charge (+0.77) and spin density (0.91) within the imidazoline ring, while the carboxylate group carried a -0.71 negative charge and low spin density (0.07). Scheme 2 illustrates the increasing positive charge and spin density in the imidazoline

Table 4. Recombination Energies of Peptide Ions

ion	recombination energy ^{a,b}		
	RE_a^c	RE_v	E_{FC}^d
h1⁺	3.30	2.39	76
h2⁺	3.18	2.30	71
h3⁺	3.32		
h4⁺	3.18		
a1⁺	3.45	2.46	88
a2⁺	3.32	2.46	71
a3⁺	3.44		
a6⁺	2.89	2.54	20
x1⁺	3.31	2.43	75
x2⁺	3.18	2.34	70
x3⁺	3.40	2.42	86

^a In units of electronvolt. ^b From averaged single point B3LYP/6-311++G(2d,p) and PMP2/6-311++G(2d,p) energies. ^c Adiabatic recombination energies include B3LYP/6-31+G(d,p) zero-point vibrational energy corrections. ^d Franck–Condon energies $E_{\text{FC}} = \text{RE}_a - \text{RE}_v$ in kJ mol^{-1} without ZPVE corrections.

ring and the increasing negative charge in the COO group as the radical system passes through **TS1** to **h2b**. Hence, the rearrangement through **TS1** can be characterized as a proton migration rather than a hydrogen atom migration.

Catalytic Effect of the Carboxyl Group. Carboxyl proton migration through **TS2** does not form a stable zwitterionic intermediate but continues by exothermic abstraction of the proximate N-3' proton by the incipient COO group forming radical **h2c**. This sequence of proton migrations accomplishes an exothermic and practically barrierless prototropic isomerization of the N-1'-H imidazole radical in **h2a** into a C-2'-H imidazoline radical in **h2c**. We note that an analogous *hydrogen atom* 1,2-migration in imidazole radicals requires a 150 kJ mol^{-1}

Scheme 2

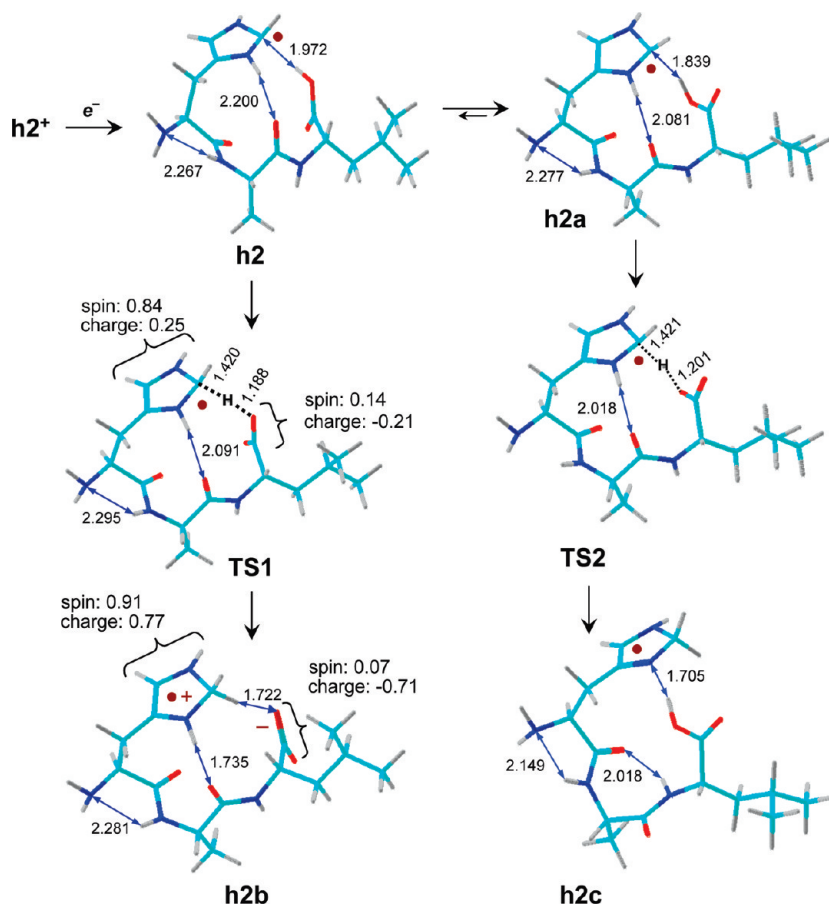


Table 5. Relative Energies of HAL Peptide Radicals

species/reaction	relative energy ^{a,b}			
	B3LYP 6-31++G(d,p)	B3LYP 6-311++G(2d,p)	PMP2 6-311++G(2d,p)	B3-PMP2 6-311++G(2d,p)
h1	0	0	0	0
h2	8	11	5	8
h3	7	11	-12	-0.3
h4	12	15	8	12
h2 → h2a	-10	-10	-16	-13
h2 → TS1	-14	-11	-27	-19
h2a → TS2	-4	-1	-11	-6
h2 → h2b	-20	-16	-11	-14
h2 → h2c	-86	-85	-70	-77
h1 → TS3	40	40	41	40
h1 → h1a	-10	-7	-16	-11
h1a → TS4	-3	-1	-9	-5
h1 → h1b	-70	-66	-58	-62

^a In units of kJ mol⁻¹. ^b Including B3LYP/6-31++G(d,p) zero-point vibrational energies and referring to 0 K.

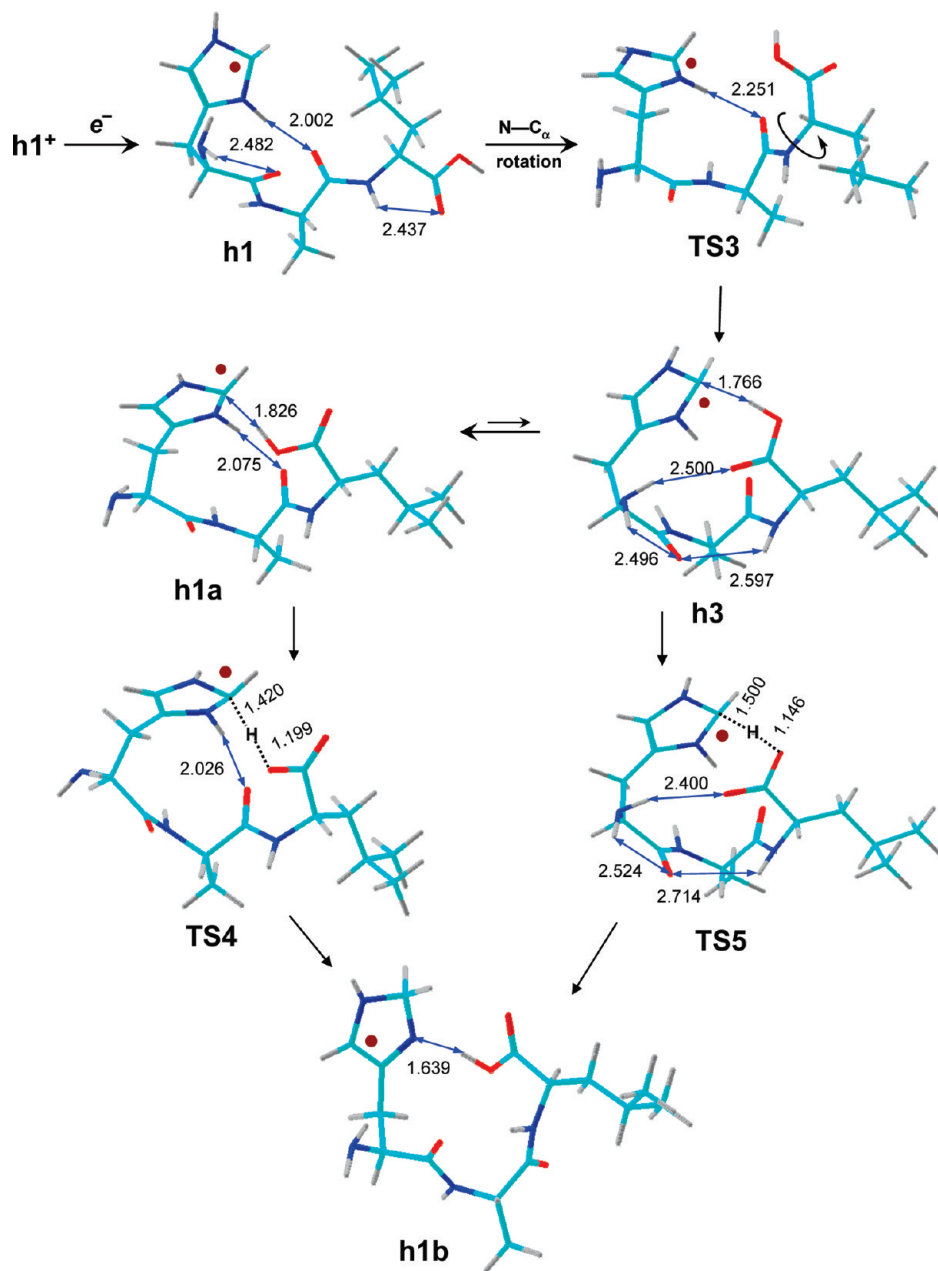
energy barrier.¹⁴ The facile isomerization of **h2a** is due to the catalytic effect of the carboxyl group which functions as a proton donor in the COOH form and a proton acceptor in the COO form. Analogous catalyzed isomerizations have been reported for ion–molecule complexes in dissociating gas-phase ions.⁴⁰ The prototropic isomerization in radical **h2a** can be viewed as an *autocatalytic process* analogous to enzymatic acid–base catalyzed reactions involving His and acidic residues.⁴¹ For example, in serine proteases a His-Asp couple acts as a proton acceptor–donor in the catalytic center and the proton transfer

involves the imine N–H bonds.⁴² In contrast, the isomerization in gas-phase His peptide radicals involves the C-2' and imine protons and is autocatalytic in that the proton transfer occurs directly between acceptor and donor sites of the His ring without participation of a substrate. One can conceive that in a peptide system of a favorable secondary structure, the first COOH → C-2' proton transfer could trigger a proton migration relay to cooperatively transport a proton to an acceptor group which may be spatially remote from the initial proton transfer site.

- (40) (a) Tureček, F.; Drinkwater, D. E.; McLafferty, F. W. *J. Am. Chem. Soc.* **1990**, *112*, 993–997. (b) Bohme, D. K. *Int. J. Mass Spectrom. Ion Processes* **1992**, *115*, 95–110. (c) Mourguès, P.; Audier, H. E.; Leblanc, D.; Hammerum, S. *Org. Mass Spectrom.* **1993**, *28*, 1098–1100. (d) Audier, H. E.; Leblanc, D.; Mourguès, P.; McMahon, T. B.; Hammerum, S. *J. Chem. Soc. Chem. Commun.* **1994**, 2329–2330. (e) Audier, H. E.; Fossey, J.; Mourguès, P.; McMahon, T. B.; Hammerum, S. *J. Phys. Chem.* **1996**, *100*, 18380–18386. (f) Gauld, J. W.; Audier, H.; Fossey, J.; Radom, L. *J. Am. Chem. Soc.* **1996**, *118*, 6299–6300. (g) Gauld, J. W.; Radom, L. *J. Am. Chem. Soc.* **1997**, *119*, 9831–9839. (h) Trikoupis, M. A.; Terlouw, J. K.; Burgers, P. C. *J. Am. Chem. Soc.* **1998**, *120*, 12131–12132. (i) Fell, L. M.; Ruttink, P. J. A.; Burgers, P. C.; Trikoupis, M. A.; Terlouw, J. K. *Int. J. Mass Spectrom.* **2000**, *195/196*, 85–99. (j) Audier, H. E.; Mourguès, P.; van der Rest, G.; Chamot-Rooke, J.; Nedev, H. *Adv. Mass Spectrom.* **2001**, *15*, 101–121. (k) Trikoupis, M. A.; Burgers, P. C.; Ruttink, P. J. A.; Terlouw, J. K. *Int. J. Mass Spectrom.* **2002**, *217*, 97–108. (l) Wong, C. Y.; Ruttink, P. J. A.; Burgers, P. C.; Terlouw, J. K. *Chem. Phys. Lett.* **2004**, *387*, 204–208. (m) Trikoupis, M. A.; Ruttink, P. J. A.; Burgers, P. C.; Terlouw, J. K. *Eur. J. Mass Spectrom.* **2004**, *10*, 801–811. (n) Wong, C. Y.; Ruttink, P. J. A.; Burgers, P. C.; Terlouw, J. K. *Chem. Phys. Lett.* **2004**, *390*, 176–180. (o) Lee, R.; Ruttink, P. J. A.; Burgers, P. C.; Terlouw, J. K. *Int. J. Mass Spectrom.* **2006**, *255*–256, 244–250.

- (41) Schneider, F. *Angew. Chem., Int. Ed. Engl.* **1978**, *17*, 583–592.
(42) Kraut, J. *Annu. Rev. Biochem.* **1977**, *46*, 3311–358.

Scheme 3



The different course of the $\text{COOH} \rightarrow \text{C-2'-H}$ migration in **h2** and **h2a** can be ascribed to the different geometries of the pertinent transition states and different hydrogen bonding of the imidazole the N-3'-H group in the incipient intermediates. In **TS1**, the forming COO group points away from N-3'-H, which is protected by forming a hydrogen bond to the Ala-amide oxygen. Both these features make the N-3'-H proton less accessible to the COO group. Note that the N-1'-H bond is too remote to be accessible for transfer to the COO group in **TS1** and **h2b**.

The major radical isomer **h1** must first undergo a conformational transformation to reach a transition state for carboxyl proton migration. Such a conformational change can proceed through **TS3** involving rotation about the Ala-Leu $\text{N}-\text{C}_\alpha$ bond as a reaction coordinate. The product of this rotation (**h3**) can isomerize by COOH group rotation to the more stable rotamer **h1a** (Scheme 3). Carboxyl proton migration onto C-2' is facile in both **h1a** and **h3** and requires practically no activation energy

in the pertinent transition states, **TS4** and **TS5**, respectively. The imidazoline product (**h1b**) is a conformer of **h2c** (shown in Scheme 2).

The important feature of the rearrangements shown in Schemes 2 and 3 is that they convert imidazole radicals **h1–h4** to imidazoline radicals **h1b** and **h2b**, their conformers, and tautomers that all have substantial electron affinities for collisional electron transfer to yield stable anions. Table 6 shows that **h1b**, **h2b**, and **h2c** can capture an electron in a bound state and therefore represent plausible intermediates for the stable anions detected in the ${}^+\text{CR}^-$ mass spectra. In contrast, the vertical electron affinities of **h1** and **h2**, pertinent to collisional electron transfer, are all negative and, thus, these radicals cannot form stable anions. The anions formed by electron transfer to imidazoline radicals **h1b** and **h2c** spontaneously rearranged upon geometry optimization to the more stable carboxylate anions, as shown for **h2c⁻** (Scheme S2, Supporting Information). Thus, we presume that the anions detected in the ${}^+\text{CR}^-$ spectra have

Table 6. Electron Affinities of Peptide Radicals

radical	electron affinity ^{a,b}	
	RE _a ^c	RE _v
h1		-0.62
h2		-0.65
h1b	2.32	0.52
h2b		1.68
h2c	3.04	0.52
a1		-0.75
a2		-0.66
a3c	2.51	0.60
a3d	3.00	2.04
x1c	1.28	0.28

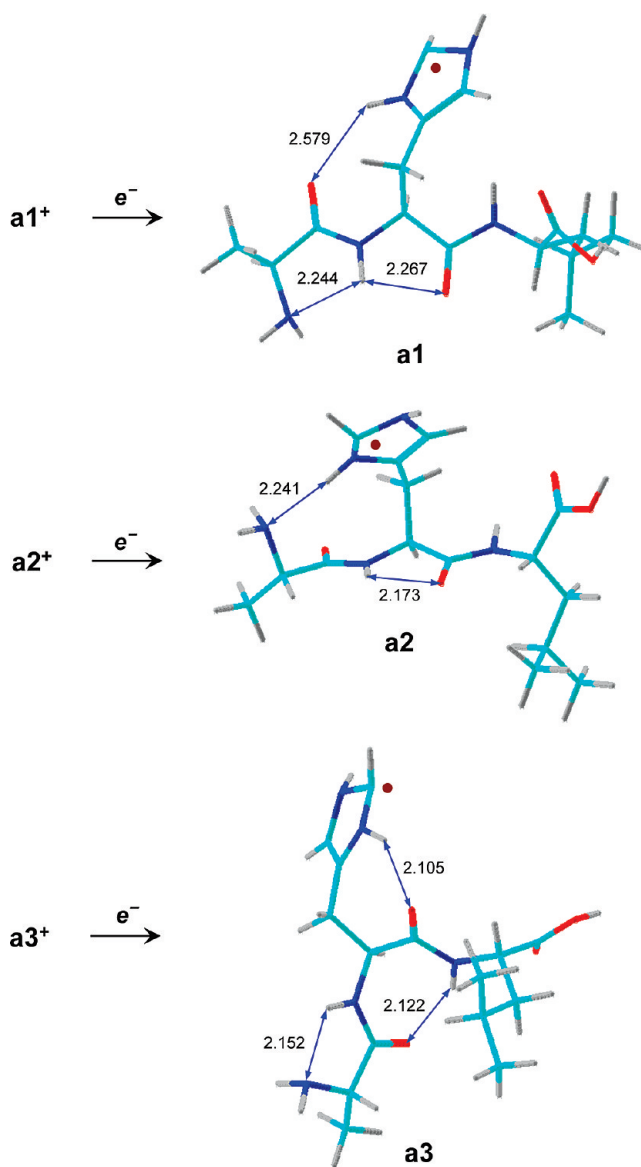
^a In units of electron volts. ^b From averaged single point B3LYP and PMP2/6-311++G(2d,p) calculations. ^c Adiabatic electron affinities include B3LYP/6-311++G(d,p) zero-point corrections.

negatively charged carboxylate groups and neutral 2'-(H) imidazoline rings.

AHL Radical Structures and Isomerizations. Electron transfer to the lowest energy AHL ion conformers **a1**⁺–**a3**⁺ forms radicals **a1**–**a3**, which are local energy minima that largely retain the hydrogen bonding pattern of the precursor ions (Scheme 4). Imidazole ring puckering and weakening of hydrogen bonds to the backbone amide groups caused by electron transfer are again the common features of **a1**–**a3**. The relative energies for AHL radicals are summarized in Table 7. The noteworthy feature of **a1**–**a3** is that they do not contain COOH groups in the proximity of the imidazole ring for proton transfer onto C-2'. The transfer can be accomplished after conformational changes consisting of consecutive or coupled bond rotations about the Leu N–C_α and His C_α–C_β bonds, as well as COOH and imidazole ring rotations. These were studied for **a3** as a representative system and found to have transition state energies ranging from 6 kJ mol^{−1} for the COOH rotation to 25 kJ mol^{−1} for the rotation about the Leu N–C_α bond. The pertinent geometries for the rotation transition states (**TS6**–**TS8**) are given in Tables S42–S44 (Supporting Information). Depending on the orientation and coupling of these internal rotations, **a3** can isomerize to conformers **a3a** or **a3b** in which the COOH groups are close to C-2' (Scheme 5). Note that in the projection shown in Scheme 5, the carboxyl OH group is pointing toward the viewer in **a3a** and away in **a3b**. These rotational isomerizations are practically thermoneutral (Table 5). Proton migrations from COOH onto C-2' have practically zero activation energies in **TS9** and **TS10** to exothermically form intermediates **a3c** and **a3d**, respectively. Species **a3c** has a C-2'-H radical imidazoline ring, whereas **a3d** is a zwitterion in which the COO anion is hydrogen-bonded to the C-2' imidazoline cation radical. Both **a3c** and **a3d** have substantial electron affinities facilitating formation of the stable anions **a3c**[−] and **a3d**[−], respectively (Table 6).

The CR spectrum of AHL shows **z₁**[−] and **z₂**[−] fragments that presumably originate from N–C_α bond dissociations in the radical intermediates. N–C_α bond cleavage can occur in a π^* excited electronic state,⁴³ according to the Utah–Washington mechanism,⁹ or in aminoketyl radical intermediates produced by migration of a histidine proton to one of the amide oxygens.¹⁴

Among the AHL radicals, **a1** has a favorable conformation for isomerization to aminoketyl radical **a1a**. The isomerization is 13 kJ mol^{−1} endothermic (Table 7) and must overcome an energy barrier in the transition state. The latter was not computed for the **a1** → **a1a** reaction, but the TS can be estimated to be 50–60 kJ mol^{−1} above **a1** by analogy with isomerizations in

Scheme 4

other histidine radicals.¹⁴ N–C_α bond cleavage in **a1a** proceeds through **TS11**, which is 43 kJ mol^{−1} above **a1** and connects **a1a** to dipole–dipole complexes of the incipient **c₁** and **z₂** fragments, for example, **a1b** (Scheme S3, Supporting Information). The overall dissociation of **a1** to **c₁** and **z₂** fragments is 16 kJ mol^{−1} endothermic. Note, however, that B3LYP energies pointed to an exothermic dissociation and differed from the MP2 dissociation energy by 38 kJ mol^{−1} (Table 7).

Electron transfer to the N-terminally protonated tautomer **a6**⁺ was calculated to give an ammonium radical (**a6**), which was 63 kJ mol^{−1} less stable than **a1** (Table 7). Radical **a6** is expected

- (43) (a) Sobczyk, M.; Anusiewicz, I.; Berdys-Kochanska, J.; Sawicka, A.; Skurski, P.; Simons, J. *J. Phys. Chem. A* **2005**, *109*, 250–258. (b) Syrstad, E. A.; Tureček, F. *J. Am. Soc. Mass Spectrom.* **2005**, *16*, 208–224. (c) Anusiewicz, I.; Berdys-Kochanska, J.; Simons, J. *J. Phys. Chem. A* **2005**, *109*, 5801–5813. (d) Anusiewicz, I.; Berdys-Kochanska, J.; Skurski, P.; Simons, J. *J. Phys. Chem. A* **2006**, *110*, 1261–1266. (e) Sobczyk, M.; Simons, J. *Int. J. Mass Spectrom.* **2006**, *253*, 274–280. (f) Sobczyk, M.; Simons, J. *J. Phys. Chem. B* **2006**, *110*, 7519–7527. (g) Skurski, P.; Sobczyk, M.; Jakowski, J.; Simons, J. *Int. J. Mass Spectrom.* **2007**, *265*, 197–212. (h) Sobczyk, M.; Neff, D.; Simons, J. *Int. J. Mass Spectrom.* **2008**, *269*, 149–164.

Table 7. Relative Energies of AHL Peptide Radicals

species/reaction	relative energy ^{a,b}			
	B3LYP 6-31++G(d,p)	B3LYP 6-31++G(2d,p)	PMP2	B3-PMP2 6-311++G(2d,p)
a1	0	0	0	0
a2	14	14	3	9
a3	2	3	5	4
a6	65	70	55	63
a3a	4	6	3	5
a3b	-0.5	3	-4	-1
a3c	-53	-51	-46	-49
a3d	-19	-16	-21	-18
a3 → TS6	6	6	6	6
a3 → TS7	14	14	15	15
a3 → TS8	25	25	25	25
a3 → TS9	-2	3	-4	-1
a3 → TS10	-7	-2	-21	-11
a1 → a1a	18	20	7	13
a1 → TS11	48	48	39	43
a1 → a1b	-42	-42	-36	-39
a1 → c₁ + z₂	2	-3	35	16
a6 → TS12	-2	-2	14	6

^a In units of kJ mol⁻¹. ^b Including B3LYP/6-31+G(d,p) zero-point vibrational energies and referring to 0 K.

to undergo a very facile loss of ammonia which requires only 6 kJ mol⁻¹ in the transition state (**TS12**, Scheme S4, Supporting Information). However, loss of ammonia is practically absent in the ⁺CR⁻ spectrum of (AHL + H)⁺ (Figure 1b). This indicates that ion **a6**⁺ is either not significantly populated among the His-protonated AHL ions or has a very low cross section for endothermic electron transfer from Cs so that the formation of radical **a6** is disfavored.

ALH Radical Structures and Isomerizations. The most stable ion conformers **x1**⁺–**x3**⁺ were used as precursors for radicals formed by electron transfer. The relative energies for ALH radicals are shown in Table 8. Radicals **x1**–**x3** that retain the main hydrogen bonding framework of their ion precursors show puckered histidine rings and weakened hydrogen bonding to the amide groups (Scheme 6). A conspicuous feature of all ALH radical conformers is that the C-2' position of the His ring cannot reach to the COOH proton without imposing a major structural distortion of the bond angles. This basically prevents an N-1'-H imidazole → C-2'-H imidazoline isomerization with the involvement of the carboxyl proton. However, we find that the carboxyl proton can interact with the imidazole C-4' and C-5' positions.

Proton transfer to C-4' was studied for **x1** where it can proceed through **TS13** to yield an imidazoline tautomer (**x1a**, Scheme 7). The latter can be characterized as a zwitterion having 94% of spin density and +0.85 charge confined within the C-4'-H imidazoline ring and a -0.76 negative charge but no spin density in the carboxyl group. However, the proton transfer to C-4' required 61 kJ mol⁻¹ in **TS13**, and isomer **x1a** was 36 kJ mol⁻¹ less stable than **x1**. An energetically more favorable isomerization was found to proceed by carboxyl proton migration onto C-5' which required 50 kJ mol⁻¹ in **TS14** (Scheme 7). The C-5'-H imidazoline intermediate (**x1b**) was 11 kJ mol⁻¹ more stable than **x1** making the rearrangement mildly exothermic. Isomer **x1b** again showed a charge distribution that pointed to its zwitterionic nature, as 96% of spin density and +0.84 charge resided in the imidazoline ring whereas the carboxyl group carried -0.77 charge and no spin density. Zwitterion **x1b** can undergo a further stabilizing rearrangement by N-H → OOC proton migration forming C-5'-H imidazoline radical **x1c**, which was 58 kJ mol⁻¹ more stable than **x1**.

Radical **x1c** was calculated to have a positive electron affinity (Table 6) and can serve as a plausible precursor for the anion

detected in the CR spectrum. An interesting feature of electron transfer to **x1c** is that the vertically formed anion undergoes spontaneous proton migration from the COOH group to the imine nitrogen. However, the thus formed imidazoline ring cannot achieve a classical π -electronic structure but is forced to be an ylid, as evidenced by its puckered geometry and pyramidization at C-2' and C-4' (Scheme 7). Imidazole ylids are known to exist as reactive intermediates in solution,⁴⁴ and simple heterocyclic ylid ions have been generated in the gas phase.⁴⁵ However, peptide ylid intermediates are unprecedented.

Isomerization Kinetics. The analysis of potential energy surfaces revealed some common features for HAL, AHL, and ALH radicals. First, there are several conformers in each group that have very similar energies and are able to interconvert by internal rotations. The nature of these rotations depends on the peptide sequence which determines the interactions between the side chain groups and thus the rotational barriers. The importance of the rotational barriers is particularly high for HAL and AHL radicals, because their rearrangements by carboxyl proton migration onto the C-2' position of the His ring show negligible energy barriers. We note that these barriers are so low that the rise of the potential energy in the TS is overcompensated by the decrease of the zero-point vibrational energy caused by the loss of the carboxyl O–H stretch, resulting in a negative barrier in **TS1**, **TS2**, **TS4**, **TS9**, and **TS10** (Tables 5 and 7). When the COOH···C-2' interaction is prevented by steric factors, migrations to the C-4' and C-5' positions of the His ring show moderate energy barriers (**TS13** and **TS14**, Table 8).

We used RRKM calculations on the B3-PMP2/6-311++G(2d,p) potential energy surface to assess unimolecular rate constants for the rearrangements. The rate constants are important for connecting the electron structure calculations to the ⁺CR⁻ mass spectra that present dissociations taking place on an experimental time scale of $t = 120$ –240 ns. Thus, only processes that have commensurate rate constants, $k \geq 1/t = 4$ –8 × 10⁶ s⁻¹ are kinetically relevant.

Figure 6 shows the calculated rate constants for the rotation about the Leu N–C_α bond, which connects **h1** with **h1a** through **TS3** (k_{rot}), and for the COOH → C-2' migration (k_{mig}). As expected, the migration becomes very fast ($k_{\text{mig}} > 10^9$ s⁻¹) within a few kJ mol⁻¹ of the TS energy. The rotation shows a shallower rise of k_{rot} and represents the rate determining step of the isomerization. We consider that about 50% of the radicals rearrange within 120–240 ns to imidazoline intermediates to give rise to stable anions detected in the ⁺CR⁻ spectrum at a comparable relative abundance (46–48%). The pertinent RRKM rate constants for 50% conversion at 120–240 ns require the internal energy in **h1** to be at 122–132 kJ mol⁻¹ (Figure 6). This is remarkably close to the mean internal energy estimated for vertically formed **h1**, $\langle E \rangle = E_{\text{ion}} + E_{\text{FC}} = 54 + 77 = 131$ kJ mol⁻¹, where E_{ion} is the precursor ion ro-vibrational energy and E_{FC} is the Franck–Condon energy. Note that this is equivalent to **h1** having a ro-vibrational temperature of 425 K. In contrast to **h1**, the other radical conformers (**h2**–**h4**) already exist in conformations that are favorable to the COOH → C-2' migration and do not require extensive backbone rotations to

(44) (a) Arduengo, A. J., III; Harlow, R. L.; Kline, M. *J. Am. Chem. Soc.* **1991**, *113*, 361.

(45) (a) McGibbon, G. A.; Heinemann, C.; Lavorato, D. J.; Schwarz, H. *Angew. Chem., Int. Ed. Engl.* **1997**, *36*, 1478–1481. (b) McGibbon, G. A.; Hrusak, J.; Lavorato, D. J.; Schwarz, H.; Terlouw, J. K. *Chem.–Eur. J.* **1997**, *3*, 232–236. (c) Lavorato, D. J.; Dargel, T. K.; Koch, W.; McGibbon, G. A.; Schwarz, H.; Terlouw, J. K. *Int. J. Mass Spectrom.* **2001**, *210/211*, 43–57. (d) Dargel, T. K.; Koch, W.; Lavorato, D. J.; McGibbon, G. A.; Terlouw, J. K.; Schwarz, H. *Int. J. Mass Spectrom.* **1999**, *185/186/18*, 925–933.

Scheme 5

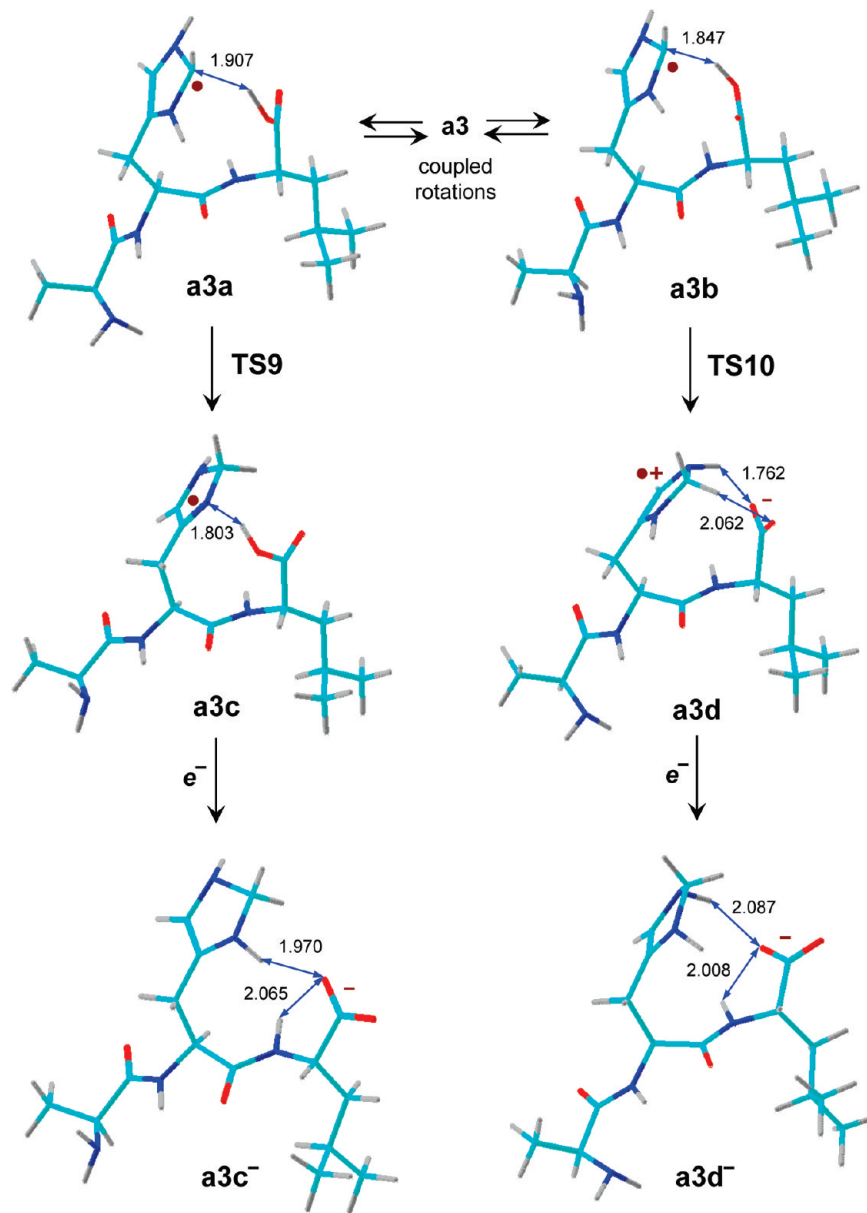


Table 8. Relative Energies of ALH Peptide Radicals

species/reaction	relative energy ^{a,b}			
	B3LYP 6-31++G(d,p)	B3LYP 6-311++G(2d,p)	PMP2 6-311++G(2d,p)	B3-PMP2 6-311++G(2d,p)
x1	0	0	0	0
x2	15	14	12	13
x3	-3	-3	-8	-5
x1a	31	34	37	36
x1b	-15	-11	-10	-11
x1c	-62	-61	-55	-58
x1 → TS13	58	60	63	61
x1 → TS14	44	47	53	50

^a In units of kJ mol⁻¹. ^b Including B3LYP/6-31+G(d,p) zero-point vibrational energies and referring to 0 K.

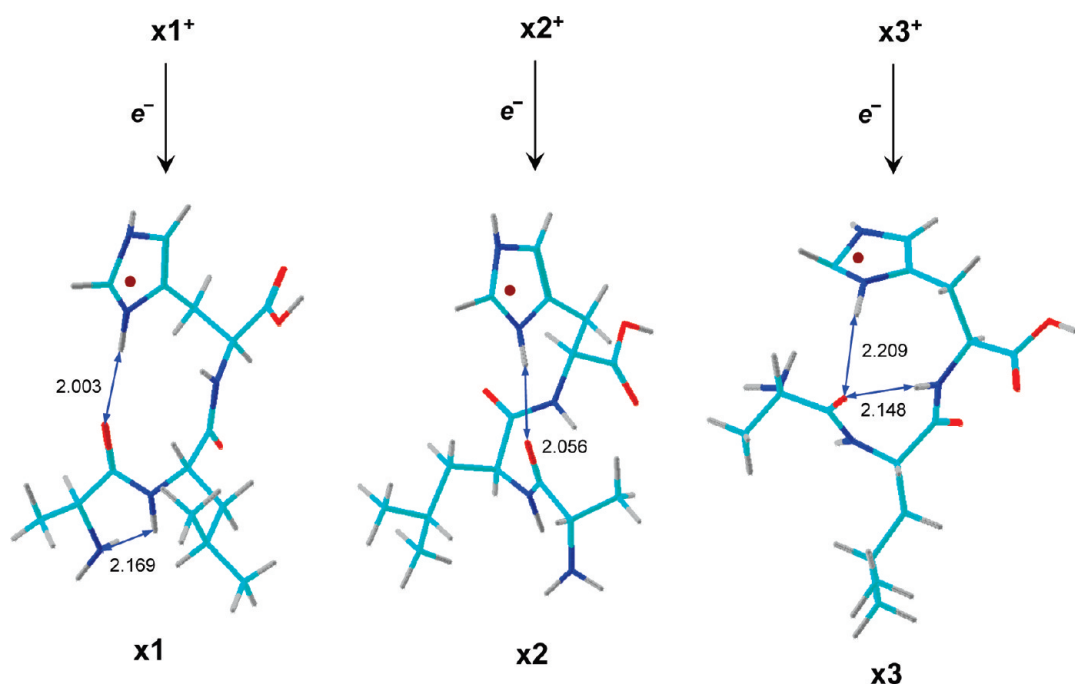
achieve the pertinent TS. These conformers presumably also contribute to the formation of imidazoline radicals that yield stable anions upon electron transfer. However, the calculated precursor ion free energies prefer **h1**⁺ as a major conformer

(Table 1), indicating that the majority of radicals formed by electron transfer should be **h1**.

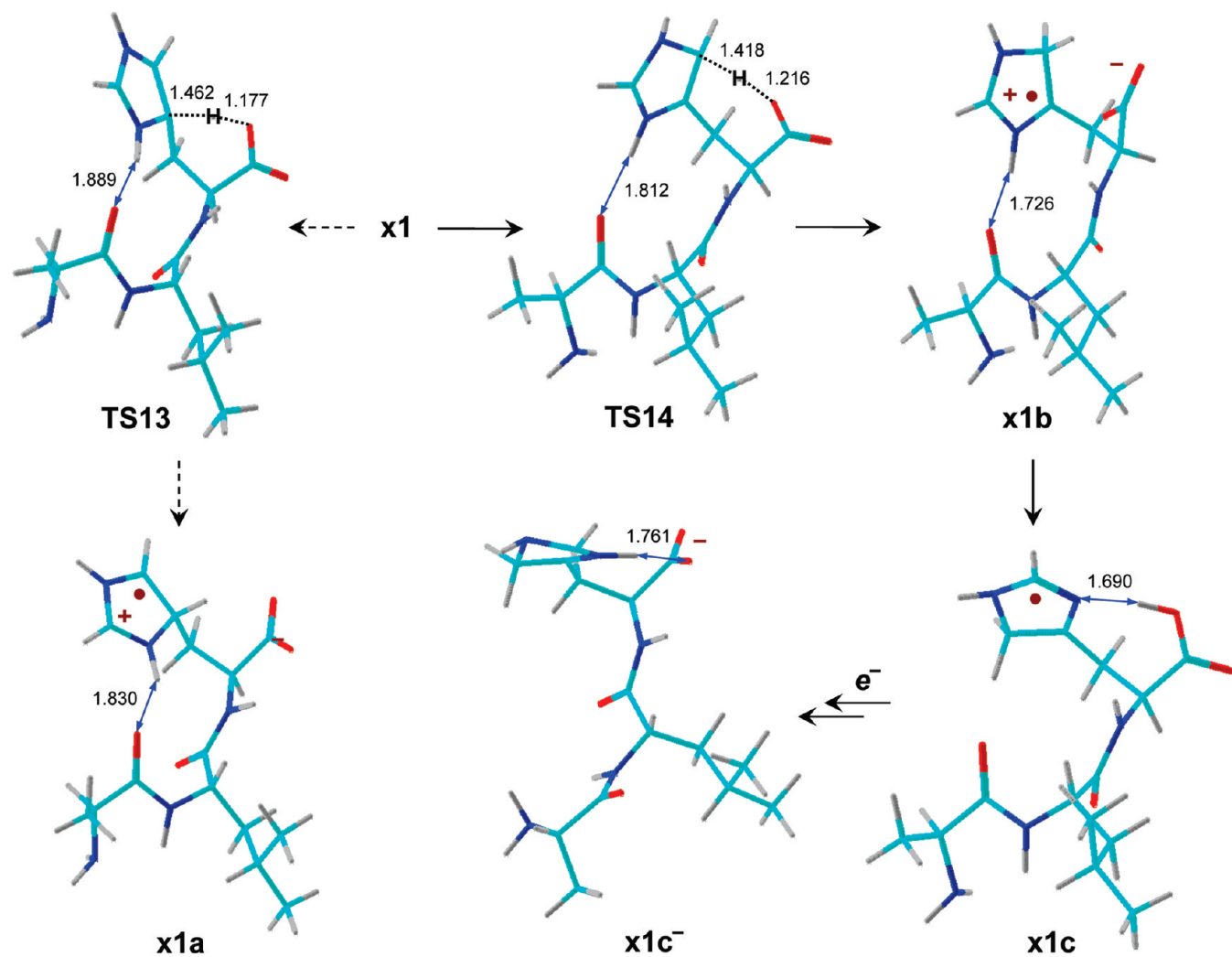
Kinetic analysis of isomerizations in the AHL system is made complicated by two factors. First, the precursor AHL ions show no particular preference among the three most stable conformers **a1**⁺–**a3**⁺ (Table 2), indicating that a mixture of radical conformers **a1**–**a3** are likely produced upon electron transfer. Second, the radicals must undergo internal rotations to reach conformations (e.g., **a3a** or **a3b**), which are favorable for the COOH → C-2' migration. In contrast to **h1**, the rotations in **a1**–**a3** are coupled in that they involve changes of 3–4 dihedral angles as internal coordinates. This makes finding the relevant transition state a daunting task. Qualitatively, the TS energies for the individual rotations (**TS6**–**TS8**, Table 7) are lower than that for **TS3** and indicate that the rotations are fast ($k_{\text{rot}} > 10^6$ s⁻¹) and can proceed on the experimental time scale to lead to the observed isomerization.

Hydrogen atom migrations in ALH radicals are of a different nature. As discussed above, the C-2' position is inaccessible to the COOH proton and cannot be directly engaged in a hydrogen

Scheme 6



Scheme 7



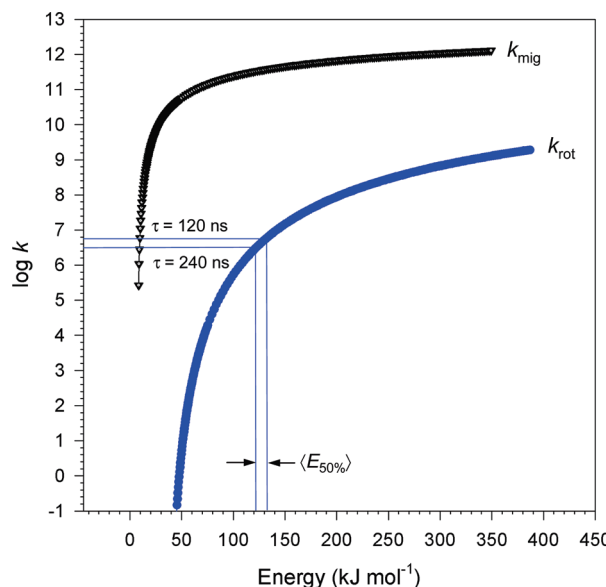


Figure 6. RRKM rate constants ($\log k, \text{ s}^{-1}$) for internal rotation (k_{rot}) in **h1** and $\text{COOH} \rightarrow \text{C-2}'$ migration (k_{mig}) in **h1a**. Vertical lines show the internal energy interval for 50% conversion on the 120–240 ns time scale.

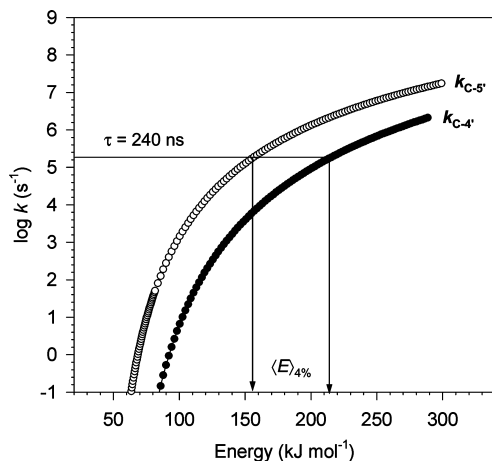


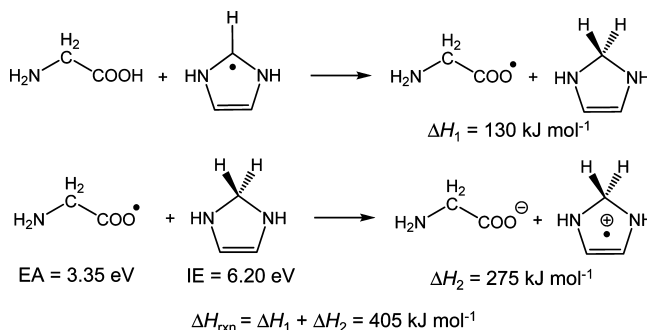
Figure 7. RRKM rate constants ($\log k, \text{ s}^{-1}$) for COOH proton migrations in **x1**; $k_{\text{C-4}'}$: migration to C-4', $k_{\text{C-5}'}$: migration to C-5'. Vertical arrows show the energy interval for 4% conversion on the 240 ns time scale.

migration. This is qualitatively consistent with the substantially lower relative abundance of the recovered anion ($\sim 4\%$) in the ${}^+ \text{CR}^-$ spectrum of ALH. RRKM analysis of proton migrations onto the C-4' and C-5' positions of the His ring is shown in Figure 7. Both rate constants, shown as $\log k(E)$, exhibit shallow slopes and reach the kinetically relevant region of $\log k = 6–7$ at high internal energies. The migration to C-5' outcompetes the other one by about an order of magnitude over the entire energy interval. Considering a 4% conversion of **x1** to **x1b** to be commensurable with the anion relative intensity in the ${}^+ \text{CR}^-$ spectrum, one gets $\langle E \rangle = 155$ and 215 kJ mol^{-1} for migrations to C-5' and C-4', respectively, to occur on a 240 ns time scale. The energy needed for the migration to C-5' is at the higher end of internal energy distribution in vertically formed **x1**, which we estimate to be centered at 140 kJ mol^{-1} . Thus, the RRKM kinetics gives a qualitatively accurate description of the isomerization and predicts the migration to C-5' to be the main channel.

Discussion

We now discuss the formation and properties of the unusual zwitterionic intermediates that play a role in the isomerizations

Scheme 8. Energies for Hydrogen Atom and Electron Transfer between Imidazoline and Carboxy Groups



of histidine peptide radicals. The thermochemistry of proton transfer from the carboxyl group to the N-1'-H imidazole radical can be broken down into two steps. The first step is a hydrogen atom transfer which can be evaluated on the basis of bond dissociation energies in simple model systems, such as 1,2(*H*)-imidazoline¹⁴ and glycine.⁴⁶ The second step is an electron transfer from the imidazoline moiety to the carboxyl radical (Scheme 8). The energy data in Scheme 8 indicate that the overall reaction between isolated carboxylic acid and imidazoline molecules is highly endothermic (405 kJ mol^{-1} for the model systems) and would not proceed without strong product ion stabilization. The stabilization in intermediates **h2b**, **a3d**, and **x1a** stems from attractive Coulomb effects of the proximate charged groups. A simple two point-charge system gains 405 kJ mol^{-1} stabilization, as negative potential energy, at a charge distance of 3.43 Å . Although a point charge model would be a gross oversimplification for the peptide zwitterions, the intramolecular distances between the highest-charged atoms are in the $2.8–3.8$ range, for example, for one of the carboxylate oxygens and the imidazoline C-2' carbon and several protons. Thus, Coulomb effects of space charge can account for the unusual stability of zwitterions **h2b**, **a3d**, and **x1a**.

In view of the low or absent barriers to the $\text{COOH} \rightarrow \text{C-2}'$ proton migration, it is somewhat surprising that the radicals undergo N–C_α bond cleavage, which requires a substantial energy barrier for the proton migration to reach an aminoketyl intermediate, for example, **a1** → **a1a** (Scheme S3, Supporting Information). The histidine hydrogen atom migration and bond rotations are unlikely to occur competitively on the same potential energy surface of the ground state **a1**, because the pertinent rate constants favor the rotation by >2 orders of magnitude. However, proton migration may be competitive in excited electronic states of vertically reduced **a1**. Figure 8 shows the six lowest electronic states in vertically formed **a1**, which fall within a 0.5 eV energy interval. In particular, the low lying A state has most of the electron density in the carbonyl groups. The pertinent molecular orbital consists of a superposition of amide and carboxyl π^* orbitals, while the planar His ring retains most of the positive charge. This electron distribution should favor proton transfer from the protonated imidazole ring onto the highly basic amide oxygen; the transfer is 103 kJ mol^{-1} exothermic to form aminoketyl radical **a1a**. Presumably, the proton transfer competes with conformational changes by internal rotations in the A state of **a1**. The initial conformation of the A state should favor transfer to the proximate, hydrogen bonded, Ala amide oxygen to form aminoketyl radical **a1a**. N–C_α cleavage in **a1a** then leads to the z_2 fragment observed in the ${}^+ \text{CR}^-$ spectrum. The rate constant (k) for the N–C_α bond

(46) (a) Yu, D.; Rauk, A.; Armstrong, D. A. *J. Am. Chem. Soc.* **1995**, *117*, 1789–1796. (b) Armstrong, D. A.; Rauk, A.; Yu, D. *J. Chem. Soc., Perkin Trans 2* **1995**, 553–560.

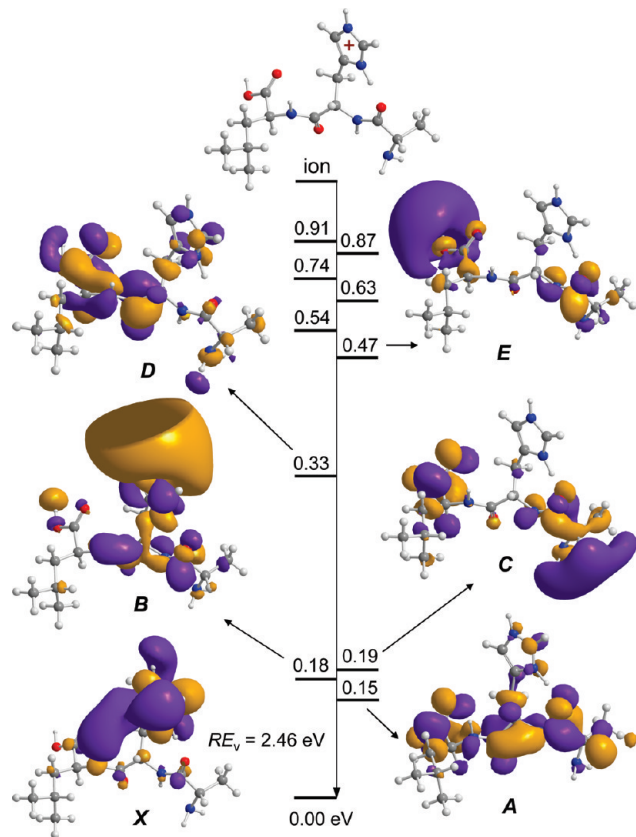


Figure 8. Electronic states in (AHL + H) radical **a1** formed by vertical electron transfer. The orbital phases are distinguished by purple and gold color.

cleavage step in the reaction sequence (**A**)**a1** → **a1a** → **TS11** → **c₁** + **z₂**, indicates that this process is kinetically feasible ($k = 1.2 \times 10^8 \text{ s}^{-1}$ at 103 kJ mol⁻¹ excitation acquired by **a1a**, Figure S3, Supporting Information). Competitive backbone rotation in the **A** state can bring the imidazolium proton close to the His amide and carboxyl carbonyl groups to facilitate transfer and result in the formation of the pertinent aminoketyl

intermediates. N–C_α cleavage in the latter can account for the formation of the **z₁** fragment. The ${}^{+}\text{CR}^-$ spectrum of AHL shows a 2:1 **z₂/z₁** ratio indicating that the proton transfer in vertically formed **a1** is faster than the backbone rotation.

Conclusions

Analysis of peptide radicals formed by collisional electron transfer in the gas phase reveals a prototropic rearrangement involving the COOH group and C-2' of the His imidazole ring. The rearrangement is virtually barrierless and is kinetically controlled by internal rotations in peptide radicals allowing them to assume conformations that are suitable for proton transfer onto C-2'. When the C-2' position is sterically inaccessible, as in ALH, the rearrangement occurs to a much lesser extent and instead proceeds to the C-5' position. C-terminal amidation of the HAL peptide eliminates this possibility thus resulting in practically no negative ion formation.

Acknowledgment. F.T. acknowledges support by the National Science Foundation (Grants CHE-0750048 for experiments and CHE-0342956 for computations). The Department of Chemistry Computer Facility has been jointly supported by the NSF and University of Washington. He also thanks the Department of Physics and Astronomy at Aarhus University, Denmark, for a Visiting Professor fellowship in July 2008 during which the above-described experiments were carried out. Research at Aarhus University was supported by the Danish Natural Research Council (Grant 272-06-0427), Carlsbergfondet (Grant #2006-01-0229), and Lundbeckfonden. Research at the German Cancer Research Center was supported by the Deutsche Forschungsgemeinschaft, the German Cancer Research Center and the Landesstiftung Baden-Württemberg. B.P. thanks the Deutsche Forschungsgemeinschaft for a Heisenberg Fellowship. B.B. thanks the DKFZ for a Guest Scientist Fellowship.

Supporting Information Available: Complete refs 22 and 24, Figures S1–S3, Schemes S1–S4, and Tables S1–S60 with optimized geometries and total energies. This material is available free of charge via the Internet at <http://pubs.acs.org>.

JA9050229